

NWP SAF

Satellite Application Facility for Numerical Weather Prediction

Document NWPSAF-EC-VS-010

Version 1.0

January 2007

Towards the assimilation of satellite microwave observations over land: feasibility studies using SSMI/S, AMSU-A and AMSU-B

Fatima Karbou, Niels Bormann, Jean-Noël Thépaut*

** CNRM-GAME, Météo-France, 42 avenue de Coriolis, 31057, Toulouse, France
European Centre for Medium-Range Weather Forecasts*



Towards the assimilation of microwave observations over land: feasibility studies using SSMI/S, AMSU-A and AMSU-B

Fatima Karbou, Niels Bormann and Jean-Noël Thépaut*

** CNRM-GAME, Météo-France, 42 avenue de Coriolis, 31057, Toulouse,
France*

European Centre for Medium-Range Weather Forecasts

This documentation was developed within the context of the EUMETSAT Satellite Application Facility on Numerical Weather Prediction (NWP SAF), under the Cooperation Agreement dated 16 December, 2003, between EUMETSAT and the Met Office, UK, by one or more partners within the NWP SAF. The partners in the NWP SAF are the Met Office, ECMWF, KNMI and Météo France.

Abstract

Satellite microwave observations are still not fully used over land within assimilation systems in spite of their large information content. So far, only observations that receive the least contribution from the surface are assimilated. Feasibility studies have been conducted within the ECMWF assimilation system as preliminary steps to extend the use of microwave data to the land surface.

This study reports on 4D-VAR experiments conducted to improve the assimilation of temperature sounding observations from SSMI/S over land. To do so, land surface emissivity and/or skin temperature have been determined using brightness temperatures from a selection of window channels, and the estimates subsequently used to assimilate data for higher frequency channels. Moreover, and prior to the assimilation experiments, land emissivities have been calculated using all SSMI/S surface channels and compared with emissivities derived from surface channels from SSMI, TMI, AMSRE, AMSU-A and AMSU-B in order to check the consistency of SSMI/S surface observations. In addition to SSMI/S experiments, other assimilation experiments have also been performed to assimilate AMSU humidity and temperature sounding channels over land.

For all assimilation experiments, the RTTOV simulations are improved when updated land emissivities are used and the assimilation system benefits from a larger number of observations compared to the control. The impact on forecast scores is positive for the Southern Hemisphere and neutral for the Northern Hemisphere when assimilating SSMI/S temperature sounding observations over land and sea. A similar impact was observed for an experiment that updates the emissivity calculations for AMSU-A and AMSU-B over land.

1. Introduction

Satellite observations are now felt to be of primary importance for numerical weather prediction (NWP). Their use in NWP has substantially advanced in the past two decades thanks to improvements in both satellite instrumentation and assimilation techniques. Efforts are made at many NWP centres in order to assimilate many more observations from relevant satellite sensors such as the advanced microwave sounding unit (AMSU) and the Special Sensor Microwave Imager (SSM/I). On the 18th October 2003, the Defense Meteorological Satellite Program (DMSP) F-16 satellite carried the first Special Sensor Microwave Imager/Sounder (SSMIS). This sensor provides unprecedented observations of the atmospheric temperature and humidity using a conical scanning technique. However, unexpected difficulties arose during the post-launch Cal/Val program. Indeed, the SSMIS Cal/Val team showed that the instrument's sounding channels are subject to local biases related to thermal emission from the main reflector and to solar intrusions into the warm calibration targets. Subsequently, calibration corrections and data flagging schemes have been developed to reduce the instrumental biases, and assimilation of the resulting pre-processed SSMIS observations has shown promising results (Bell et al. 2007). It is worthy to mention that similar instrumental biases have been also observed while processing observations from other conical scanning instruments such as the Tropical Rainfall Measurement Mission Microwave Imager (TRMM) Microwave Imager (TMI), the Advanced Microwave Scanning Radiometer – ADEOS II (AMSR), and from SSM/I. These instruments have been carefully calibrated in order to allow an effective use of their observations for atmospheric applications.

Besides calibration issues, other issues should be examined when using SSMIS surface sensitive channels (or coming from other microwave sensors) over land. So far, the use of microwave observations from sounding channels is still more intensive over sea than over land. Their use over land is still limited to channels that receive a weak contribution from the surface. This limitation is less important over oceans for at least two reasons: (1) seas are associated with low emissivity values (close to 0.5) and high emissivity polarization differences. Moreover, (2) effective emissivity models have been developed and are accurate enough to meet the NWP requirements (Deblonde and English 2000; Guillou et al. 1998;

Prigent and Abba 1990; Guissard and Sobieski 1987; Wentz 1975; Rosenkranz and Staelin 1972). Land surface emissivities at microwave frequencies are rather high (almost 1.0) and vary in a complex way with surface types, roughness and moisture among other parameters. Recent studies have shown that alternatives to empirical emissivity modelling could help the assimilation of microwave observations that receive a strong or a weak contribution from the land surface. Prigent et al. (2005) used estimated emissivities from SSM/I and AMSU-A surface channels to prepare AMSU-A assimilation over land in the European Centre for Medium-Range Weather Forecasts (ECMWF) Forecasting System. Within the Météo-France 4D-Var system, three methods have been tested in order to assimilate the Advanced Microwave Sounder Unit-A (AMSU) and AMSU-B observations over land: (1) the first method uses averaged emissivity atlases derived from AMSU-A and -B surface channels, (2) the second one uses emissivity estimates dynamically derived for each atmospheric situation and at only one AMSU-A and AMSU-B channel, and (3) the third method is based on the first one with dynamical skin temperature estimation using one AMSU-A and AMSU-B channels (Karbou et al. 2006a). It is worth mentioning that channels that are involved in the dynamical estimation of emissivity or skin temperature are discarded from any other computation or diagnostic to ensure that the same information is not used twice during the assimilation. The land emissivity methods described above have been shown to be beneficial to RTTOV simulations. For all schemes, and by comparison to a control experiment, the brightness temperature (T_b) simulations are in better agreement with the observations. The First guess departures (observations-simulations) statistics are improved and an increase of the number of observations that could be assimilated is noticed. The three emissivity methods have also been evaluated by looking at the analysis and forecast fields (Gerard et al. 2006, Karbou et al. 2006b). All assimilation experiments that use an updated surface emissivity scheme, have shown a modification of the humidity analysis particularly beneficial to areas famous for their lack of strato-cumulus clouds like in the Guinea Gulf and also to too rainy areas (in particular Central Africa and Arabia). The African monsoon within the French 4D-Var system was seen to be displaced in the analysis and forecasts. Further experiments, with an emphasis on tropical areas, are conducted in order to derive final conclusions.

The main objective of this work is to investigate the feasibility of assimilating surface sensitive SSMI/S sounding channels over land by using emissivity land methods previously tested for AMSU-A, AMSU-B and SSM/I observations. To reach our objective two issues have been investigated: (1) land surface emissivities have been derived using SSMI/S surface channels and compared with emissivities derived from observations coming from different microwave sensors (AMSU-A, AMSU-B, SSM/I, AMSR-E, and TMI). Such comparisons are very useful for inter-sensor calibration control. The second issue is (2) to attempt the assimilation of SSMI/S observations over land in the ECMWF forecasting system and to examine the impact of these SSMI/S temperature sounding channels on the analysis and the forecast fields. Microwave observations and emissivities are described in section 2. Land emissivities and T_b s from SSMI/S are compared with emissivities and T_b s from SSM/I, TMI, AMSR-E, AMSU-A and AMSU-B in section 3. The assimilation experiments are described in section 4. Results in terms of model fit to the observations and forecast scores are given in the latter section.

2. Data and method

2.1. Microwave observations

The SSMI/S sensor represents an important advancement over its predecessor, SSM/I, as it combines the SSM/I imaging capabilities and the profiling capabilities of ancillary microwave sounders. SSMI/S allows microwave measurements at 24 frequencies ranging

from 19 to 183 GHz. SSMI/S has 14 channels in the 50-60 GHz range which allow atmospheric temperature sensing from about 80 Km down to the earth surface. In addition to temperature sounding channels, SSMI/S combines humidity sounding channels close to the strong 183 GHz water vapour line as well as imaging channels in common with SSM/I. Table 1 lists the SSMI/S channel parameter specifications and Figure 1 shows weighting functions for a standard atmosphere and for a selection of SSMI/S channels. For all experimentation reported here, we use the SSMI/S data pre-processed by the Met.Office (Bell et al. 2007). This means solar intrusion affected data is excluded, a correction is applied for the thermal emissions from the instrument's reflector, and remapping and spatial averaging is performed to provide collocated data from all channels with reduced noise characteristics.

The SSM/I is a conical scanning passive microwave imager and is onboard the latest generation of the DMSP satellites since June 1987. It allows observation acquisition at four frequencies (19.3, 22.2, 37.0 and 85.5 GHz), with a dual polarization (only horizontal at 22.2 GHz) and has a near constant zenith angle of 53°. The instrument makes measurements with a mean altitude of 830 km, a swath width of 1400 km and a horizontal resolution that varies from 12.5 km (at 85.5 GHz) to 25 km (at 19.3 GHz). For our study, SSM/I observations from DMSP F13 and F14 satellites have been used.

In addition to SSM/I observations, data from other microwave instruments have been used (AMSRE, TMI, AMSU-A and AMSU-B). The Advanced Microwave Scanning Radiometer – Earth Observing System (AMSR-E) instrument is operating aboard NASA's Aqua Satellite since 4 May 2002. It is a twelve-channel, six-frequency, passive-microwave radiometer system with a near constant zenith angle of about 55°. It measures horizontally and vertically polarized brightness temperatures at 6.9, 10.7, 18.7, 23.8, 36.5, and 89.0 GHz. At an altitude of 705 km, AMSRE measures the upwelling scene brightness temperatures with a swath width of 1445 km and a horizontal resolution that varies from 6 km (at 89 GHz) to 60 km (at 6.9 GHz).

The TMI instrument is aboard the TRMM mission since November 1997 and measures the intensity of radiation at five separate frequencies: 10.7, 19.4, 21.3, 37, 85.5 GHz. The TRMM orbit altitude is close to 400 km. As a consequence, TMI has a 760 km wide swath width with a high and variable horizontal resolution (6 km at 85.5 GHz to 50 km at 10.7 GHz) and also with an observation zenith angle ranging from about 47° to 53°.

AMSU-A & AMSU-B sounders are operating on board the latest generation of the National Oceanic and Atmospheric Administration (NOAA) polar orbiting satellites since May 1998. Moreover, the National Aeronautics and Space Administration (NASA) Aqua mission and more recently the Metop-A mission carried similar instruments (MHS for AMSU-B). AMSU-A is designed for atmospheric temperature sensing whereas the AMSU-B sounder is used for humidity probing. The AMSU-A instrument makes measurements at 15 frequencies which include 12 frequencies near the oxygen absorption band (50-60 GHz). AMSU-B makes measurements at 3 frequencies close to the strong water vapour absorption line at 183.31 GHz. In addition to sounding channels, AMSU-A & -B have the so-called "window channels" which give measurements sensitive to the surface and to low level atmospheric layers (23.8, 31.4, 50.3, 89, and 150 GHz). Both instruments observe the Earth with a scan angle that varies from -48° to +48° with respect to nadir.

In order to prepare the assimilation of SSMI/S observations over land, land emissivity calculations have been performed using SSMI/S channels that receive a strong contribution from the surface. SSMI/S land emissivities have been compared to land emissivities directly calculated using surface channels from the following microwave sensors: SSM/I, AMSRE, TMI, AMSU-A and AMSU-B. Table 2 shows surface channels from different microwave sensors that have been used for comparison purposes with SSMI/S land emissivity estimations.

2.2. Emissivity computation at microwave frequencies

Land emissivities have been calculated directly from satellite observations assuming a flat and specular surface. Several studies have been carried out to estimate land emissivities using satellite measurements (Choudhury 1993, Felde and Pickle 1995, Jones and Vonder Haar 1997, Prigent et al 1997, Morland et al. 2000-2001, Weng et al. 2001, Karbou et al. 2005 among others). In the case of a non-scattering plane parallel atmosphere and for a given path zenith angle and a microwave frequency, the T_b observed by a sensor can be expressed as:

$$(1) \quad \left. \begin{aligned} T_{b(\theta, \vartheta)} &= T_s \times \varepsilon_{(\theta, \vartheta)} \times \Gamma + (T_{atmo}^{\downarrow} \times (1 - \varepsilon_{(\theta, \vartheta)}) \times \Gamma) + T_{atmo}^{\uparrow} \\ \Gamma &= \exp \left\{ \frac{-\tau(0, H)}{\cos(\theta_z)} \right\} \end{aligned} \right\}$$

where $T_{b(\theta, \vartheta)}$ and $\varepsilon_{(\theta, \vartheta)}$ are the measured t_b and the corresponding surface emissivity, respectively, at frequency ϑ and at observation zenith angle θ . $T_s, T_{atmo}^{\uparrow}, T_{atmo}^{\downarrow}$ are the surface skin temperature, the atmospheric upwelling and downwelling temperatures respectively. Γ is the net atmospheric transmission and it is a function of the atmospheric opacity τ (between the surface and the top of the atmosphere height H) and the observation zenith angle θ . Using equation 1, the microwave land emissivity at a frequency μ and with a polarization p can be written as

$$(2) \quad \varepsilon_{(\theta, \vartheta)} = \frac{T_{b(p, \vartheta)} - T_{(\vartheta, \uparrow)} - T_{(\vartheta, \downarrow)} \times \Gamma}{(T_s - T_{(\vartheta, \downarrow)}) \times \Gamma}$$

Surface channel observations coming from SSMI/S, SSMI, TMI and AMSRE antenna systems are made with a horizontal or a vertical polarization whereas AMSU-A and AMSU-B observations are a mixture between horizontal and vertical polarizations. Emissivities with a mixed polarization could be expressed as

$$(3) \quad \begin{aligned} \varepsilon_{(\theta, \vartheta)}^{mixed} &= \varepsilon_{(\theta, \vartheta)}^p \cos^2 \varphi + \varepsilon_{(\theta, \vartheta)}^q \sin^2 \varphi \\ \varphi &= \arcsin \left(\frac{R}{R + H_{sat}} \sin \theta \right) \end{aligned}$$

where $\varepsilon_{(\theta, \vartheta)}^p$ and $\varepsilon_{(\theta, \vartheta)}^q$ are emissivities at θ and φ are emissivities at the two orthogonal polarizations. θ and φ are the satellite observation zenith and scan angles respectively. φ is expressed as a function of θ , the radius of the Earth R and the satellite height H_{sat} . For AMSU-A and AMSU-B window channels, the polarization is assumed to be vertical at nadir. As a consequence, the AMSU emissivity is written as

$$(4) \quad \varepsilon_{(\theta, \vartheta)}^{mixed} = \varepsilon_{(\theta, \vartheta)}^V \cos^2 \varphi + \varepsilon_{(\theta, \vartheta)}^H \sin^2 \varphi$$

here, $\varepsilon_{(\theta, \vartheta)}^V$ and $\varepsilon_{(\theta, \vartheta)}^H$ are emissivities at vertical and horizontal polarizations respectively.

Land emissivity calculations have been conducted over a two week period (12 to 25 August 2006) following the methodology described earlier in this section. ECMWF short range (12 h) temperature and humidity forecast profiles have been used to feed the RTTOV

radiative transfer model in order to calculate the atmospheric components needed for equation 2. Surface temperatures coming from the ECMWF short range forecasts have also been used. Emissivities have been calculated for many microwave channels coming from different microwave sensors (listed in Table 2). In order to meet the constraints of operational assimilation, no cloud clearing of the microwave observations has been performed except quality checks of the observations based on window channels. For example, SSMI/S fg-departures for channels 1-4 are used to accept or reject observations at higher frequencies. In the context of this study, the cloud contamination of microwave observations is likely to occur and could explain part of the variability of observation departures from first guess or from analysis.

3. Inter sensor comparisons

3.1. *land emissivity and Tbs comparisons*

Land emissivities derived from satellite observations are in fact “effective emissivities” integrated over the satellite foot print. In-situ emissivity measurements at large spatial scales are necessary to evaluate satellite emissivity estimates. However, due to the lack of such in-situ measurements inter sensor emissivity comparisons have been performed instead. The consistency of retrieved emissivities, in terms of spatial, frequency and angular (for AMSU-A & -B) variations, has also been checked.

Mean emissivity maps at 19 GHz at vertical polarization (V) and mean emissivity difference maps between vertical and horizontal (H) polarizations at the same frequency are shown in Figure 2 and Figure 3 respectively. These maps have been averaged using 2 weeks of observations (from 12 to 25 August 2006) from SSMI/S, SSMI, AMSRE and TMI. All averaged maps show expected spatial variation of the emissivity: desert and snow areas are associated with high emissivity polarization difference. Emissivities for forests have a small variation with the polarization. In fact, unlike desert and snow areas, dense vegetation regions are associated with a quasi-lambertian reflection. Mean emissivity maps from SSMI/S are in good agreement with SSM/I, TMI and AMSRE ones. Figure 4 completes the comparison by showing mean emissivity maps obtained at frequencies close to 91 GHz, at AMSU mixed polarization and from SSMI/S, SSM/I, AMSU-A, TMI, and AMSU-B. For conical scanning instruments, emissivities at vertical and horizontal polarizations have been used to get emissivities with a mixed polarization following equation (4). For AMSU-A and AMSU-B, only emissivities obtained at high observation zenith angles have been averaged. As expected, emissivity varies with surface types: contrarily to forests, desert and snow areas exhibit low emissivity values. Lakes and rivers are also associated with low emissivities. A rather good agreement between emissivities from all sensors can be observed.

However, SSMI/S emissivities seem to be slightly larger compared with the other instruments. In order to investigate this effect, emissivities from all sensors have been analyzed by surface types. The Biosphere-Atmosphere Transfer Scheme (BATS) datasets have been used to identify surface types (Dickinson et al. 1986) and are displayed in Figure 5. V and H emissivities from conical scan instruments have been processed using equation (4) to be compared with AMSU-A and AMSU-B emissivities. Mean AMSU-A emissivity curves with respect to 30 scan positions ($\pm 58^\circ$ of zenith angle variation) obtained at 23, 31, and 89 GHz and for tropical forests and desert are displayed in Figure 6. Emissivities coming from SSM/I, SSMI/S, AMSRE, TMI and AMSU-B are also added to the plots. Figure 6 illustrates a positive bias in SSMI/S emissivities at all frequencies compared with emissivities from other microwave sensors. The SSMI/S emissivity bias is larger at horizontal polarization and at low frequencies: almost 5% is observed over dense vegetation regions at 19-H GHz with respect to SSM/I. This bias is close to 2% over bare soils. It should be mentioned that 2-4 % of bias

in the emissivity could represent up to 5-10 K of Tb bias (assuming a skin temperature of 300 K and an atmospheric transmission of 0.9). The emissivity correlation coefficients have also been determined for SSMI/S, SSM/I, TMI and AMSRE surface channels (see Figure 7) using 2 weeks of data. We noticed a rather good agreement between emissivity correlation coefficients from SSM/I, AMSRE and TMI. The agreement is less good for SSMI/S low frequency channels. For example the correlation coefficients between emissivities at 19-V GHz and 19-H GHz are 0.62, 0.63, and 0.68 for SSM/I, TMI, and AMSRE respectively against 0.28 for SSMI/S. Correlation coefficients between channels with vertical polarization seem to be in better agreement. The correlation coefficients between emissivities at 19-V GHz and 37-V GHz are 0.93, 0.92, 0.93, and 0.92 for SSMI/S, SSM/I, TMI, and AMSRE respectively. The properties of the emissivity correlation coefficient are mainly due to Tb correlation coefficients which exhibit the same characteristics. Figure 8 shows Tb correlation coefficients obtained from the same 2 weeks of data from different microwave sensors including SSMI/S. Land and sea observations have been separated. It seems that the SSMI/S correlation coefficients are in better agreement with correlation coefficients from the other sensors over sea. Over land, the agreement is worst between channels having two different polarizations (at least for low frequencies). SSMI/S observations have been pre-processed in order to reduce the instrumental biases. The pre-processing consists of remapping and averaging (to ~ 118 km resolution) the observations as well as flagging measurements concerned by the solar intrusion problem. A reflector correction is also applied during the pre-processing stage. Once pre-processed, SSMI/S observations are smoothed. As a consequence, SSMI/S Tbs (and indirectly emissivities) experience a lesser variability especially over land. This may imply low correlation coefficients for the most sensitive SSMI/S channels to the surface. Over sea, Tbs from SSMI/S surface channels exhibit a lesser variability and are in very good agreement with SSM/I surface channel Tbs (see correlation coefficients in Figure 8). Moreover, mean SSMI/S Tbs and standard deviations computed using 4 days of sea data correspond well to SSM/I ones (see Figure 9). In addition to the effect of smoother Tbs, SSMI/S observations are flagged to remove data contaminated by the solar intrusion. As a consequence, data gaps occur over many areas and the Tb variation interval is artificially reduced. Figure 12 shows global time series of Tbs over land at 19-V GHz from SSMI/S (a) and from SSM/I (b). One can notice that SSMI/S Tbs experience a lesser variability than SSM/I because of data flagging. Consequently, mean Tb values (and emissivities) computed using only "hot" scenes are seen larger than Tbs (emissivities) from the other microwave sensors.

In addition, mean averaged SSMI/S Tbs from temperature and humidity channels have been compared with temperature and humidity Tbs from AMSU-A and AMSU-B observations close to 53° . For this comparison, only channels with no contribution from the surface have been considered. Figure 10 displays mean Tb maps averaged over two weeks and obtained at 55.5 GHz from SSMI/S (Figure 10.a) and from AMSU-A (Figure 10.b). Mean Tb maps at 183 ± 1 GHz (SSMI/S and AMSU-B) are also presented. A very good agreement between the Tb maps can be observed. Sea Tb mean curves have also been plotted against latitudes for two temperature channels (54.4 and 55.5 GHz) and for two humidity ones (183 ± 3 and 183 ± 1 GHz) coming from SSMI/S, AMSU-A and AMSU-B (not shown). Even if these observations are not perfectly collocated, a very good agreement between all Tbs can be observed. This indicates a good consistency between mean SSMI/S and AMSU observations, at least when averaged over longer periods. Monitoring of SSMI/S data against First Guess equivalents conducted by several groups also indicates that noise levels for the temperature sounding channels in the pre-processed data are comparable to those of AMSU-A, yet some considerable local biases remain (Bell et al. 2007). The SSMI/S surface channels biases and correlations are likely to be due to unexpected side effects of SSMI/S observations flagging,

remapping and averaging. Assimilation experiments using temperature sounding channels over sea and land have been conducted and will be discussed in section 4.

3.2. *Tbs simulations*

SSM/I/S Tbs over land have been simulated using the RTTOV radiative transfer model for 2 weeks (from 12 to 26 of August 2006) and for a selection of channels. The land surface emissivity has been determined using two approaches: (1) using a single constant value of 0.99 for the land surface emissivity for all channels and (2) using satellite emissivities derived at 19-V and 19-H GHz (called experiment). SSM/I/S channels with a H polarization will take the emissivity at 19-H GHz whereas the 19-V GHz emissivities will be allocated to channels with a V polarization. The differences between observed and simulated radiances using the background fields (called 'fg-departures' hereafter) have been computed for the control, and the experiment. Histograms of fg-departures obtained globally and for some SSM/I/S channels are given in Figure 11. No bias corrections have been applied for these comparisons. The results shown on Figure 11 indicate that fg-departure statistics are improved when the surface emissivities are updated using 19-V and 19-H emissivities. As expected, the improvements are quite dramatic for the surface channels, partly reflecting the otherwise very poor specification of surface emissivities based on a single constant value in approach (1). Updated emissivities are also shown to be beneficial to sounding channels (temperature and humidity) that receive a weaker contribution from the surface. In the same manner, fg-departures have also been computed for SSM/I, TMI, AMSR-E, AMSU-A, and AMSU-B. For these instruments, emissivities have been taken from low frequency channels and have been allocated to higher frequency channels. Overall, fg-departures statistics (bias and standard deviations) are well improved when the surface emissivities are updated (not shown).

It should be mentioned that the frequency dependence of the emissivity has not been taken into account for SSM/I/S Tbs simulations as emissivities at 19 GHz are attributed to higher frequency channels (including the 50-60 GHz). Ideally, a frequency parameterization should be introduced. One could also use the closest (in frequency space) surface channels to simulate Tbs at sounding frequencies. For example, emissivities at 50 GHz could be used for temperature sounding channels close to the 50-60 GHz oxygen band and emissivities could be derived at 91 GHz to help assimilating observations near the 183.31 GHz water vapour line. However, the sensitivity to the surface at 50 GHz and at 91 GHz is much lower than at 19 GHz. Figure 13 shows atmospheric transmission histograms calculated under the assumption of clear sky at 50, 91 and 19 GHz. This figure shows that the atmospheric transmission is higher than 0.9 at 19 GHz and is within 0.5-0.6 at 50 GHz. Under clear sky conditions, 100%, 84% and 83% of SSM/I/S observations have an atmospheric transmission greater than 0.5 at 19, 50 and 91 GHz respectively. Of course, these percentages are much lower in presence of clouds.

In the next section and for SSM/I/S sounding channels, the land emissivities will be derived from the closest (in frequency space) surface channels. In this case, temperature sounding (50-60 GHz) and humidity sounding channels (150 and ~183.31 GHz) will take the emissivity calculated at 50-V GHz and 91-H GHz respectively. An emissivity atlas calculated over 2 weeks prior to the assimilation period is used when the atmospheric transmissions at 50 and 91 GHz are lower than 0.5 (ie., in around 16% of cases)

4. Assimilation experiments

4.1. Overview

Following the methodologies developed for AMSU-A, AMSU-B and SSM/I (Karbou et al. 2006), three methods have been implemented in the ECMWF 4D-Var assimilation system and adapted to SSMI/S observations. (1) the first method uses averaged emissivity atlases derived from SSMI/S surface channels (19V, 19H, 22V, 37V, 37H, 50V, 91V, 91H), (2) the second one uses emissivity estimates dynamically derived for each atmospheric situation and at SSMI/S 50V, 19V, 19H, and 91H channels, and (3) the third method is based on the first one with dynamical skin temperature estimation using SSMI/S 19V. It is worth mentioning that channels that are involved with the dynamical estimation of emissivity or skin temperature are discarded from any other computation or diagnostic to ensure that the same information is not used twice during the assimilation. When the atmospheric transmission is lower than 0.5, the dynamical estimation of emissivity or skin temperature is not performed to avoid too noisy emissivity retrievals. In this case, emissivities from an atlas and surface temperature from the background are used.

The SSMI/S temperature sounding channels from the pre-processed dataset are so far the best characterised ones, with noise characteristics that are broadly comparable to AMSU-A, yet with some remaining local biases (Bell et al. 2007). For this reason, we have chosen to start with the assimilation of temperature sounding channels over land. Assimilation experiments have been run covering the period 26 August to 26 September 2006. All experiments reported here use ECMWF's 12 h incremental 4DVAR system, with a model resolution of T511 (~40 km), and an analysis resolution of T159 (~125 km), with 91 levels in the vertical up to 0.01 hPa. 10-day forecasts were performed from every 0 Z analysis. Other observations used in the system are the same as used operationally at the time. Three experiments were conducted: The control experiment (called 'SSMI/S control' hereafter) uses SSMI/S channels 2-7 and 23-24 in addition to the operational set of observations. Channels 2-4 are used over sea only. Other assimilation and quality control settings for SSMI/S for this experiment are as described in Bell et al. (2007). In addition, an experiment with emissivities dynamically estimated at 50V, 19V, 91H (method 2) and using temperature sounding observations (channels 2-7, 23-24) over land and sea has been performed (called 'experiment-dyn' hereafter). For this experiment, emissivities derived at 50V and at 91H have been used for temperature and humidity sounding channels respectively. For SSMI/S surface channels, emissivities derived at 19GHz (V & H) have been used. A third experiment (called 'experiment-skin' hereafter) that assimilates temperature sounding channels over land and sea has been run using method 3. For this experiment, the skin temperature is derived at 19-V GHz using the equation:

$$(5) \quad T_s = \frac{Tb_{19-V} - (1 - \varepsilon_{atlas})T_{(19-V,\downarrow)} - T_{(19-V,\downarrow)}}{\varepsilon_{atlas} \Gamma}$$

Where, ε_{atlas} is the averaged emissivity at 19-V GHz over 2 weeks prior to the assimilation period. Tb_{19-V} , $T_{(19-V,\uparrow)}$, $T_{(19-V,\downarrow)}$, and Γ are the 19-V Tbs, upwelling Tbs, downwelling tbs and the atmospheric transmission respectively. The skin temperature is then allocated to the remaining SSMI/S channels as a guess. Table 3 summarizes the SSMI/S assimilation experiments.

In addition to the SSMI/S experiments, other experiments have been conducted to investigate the effect of improved emissivity estimates for AMSU-A and AMSU-B

observations in the ECMWF system. In this case, the control experiment (hereinafter ‘AMSU control’) uses just the operational set of observations, without adding SSMI/S. This experiment uses a classification-based emissivity scheme that uses regressions and empirical models (Weng et al. 2001, Grody 1988) to allow assimilation of some surface-sensitive AMSU channels over land. The assimilation of surface-sensitive channels over land is restricted to AMSU-A channels 5 and 6 over low orography, and to channels 3 and 4 of AMSU-B or MHS over low orography. AMSU-A channels 1-4 and 15 are not assimilated over sea or land, and AMSU-B/MHS channel 5 is only assimilated over sea. A second experiment has been conducted by changing the land emissivity (called experiment-dyn1). For this experiment, AMSU-A emissivities derived at 31 GHz (channel2) and AMSU-B emissivities derived at 89 GHz (channel 1) have been used for the remaining AMSU-A and AMSU-B channels, respectively. See Table 4 for a summary of AMSU experiments.

In the next sections, results from all SSMI/S assimilation experiments (control, experiment-dyn, and experiment-skin) will be analyzed in terms of observation operator simulations (fg-departure statistics, number of observations used ...). The impact of SSMI/S temperature sounding channels over land in the analyses and forecasts will also be examined. The impact of updating AMSU-A & -B land emissivities will also be examined.

4.2. 4D-VAR SSMI/S assimilation results

a) Model fit to the observations

Overall, there is no divergence between the assimilation of SSMI/S observations over land and the assimilation of other observations. Indeed, the fit of other observations against the First Guess or the analysis is not altered when SSMI/S temperature observations are assimilated over land (using experiment-dyn and experiment-skin, not shown).

Figure 14 shows the statistics for the FG (solid) and the analysis departures (dashed) for the assimilated SSMI/S observations within the control (red) and the experiment-dyn (black). Results are given in terms of standard deviations, biases and number of assimilated observations. For SSMI/S observations, adding channels 2, 3, and 4 over land results in an increase of up to 93% in the number of used observations with respect to the SSMI/S control over the Northern Hemisphere for these channels. Many more data are not rejected over land when the surface emissivity is constrained by channel 1 (50GHz). Note that the experiments use a check on the First Guess departures of channel 2 (absolute departures should be below 0.7 K) to identify data with too strong cloud contamination for channels 2-4. As channel 2 is quite sensitive to the surface, the updated emissivities will have an impact on the data considered cloudy over land. Some degradation of the bias and the standard deviation for channels 2 is observed when assimilating SSMI/S temperature sounding observations over land (for experiment-dyn and experiment-skin), suggesting that the data shows larger First Guess departures over land than over sea. Nevertheless, the fg-departure global statistics for channels 3 and 4 are acceptable and are not degraded over land. Figure 15 shows mean global bias and standard deviation maps for SSMI/S channel 3 fg-departures obtained from experiment-dyn. No specific bias or variability features can be noted over land compared with sea. It should be mentioned that the bias correction has been done using the same predictors over land and over sea. At least for channels that receive a contribution from the surface, the bias correction seems to be less successful over land than over sea.

Considering data over land only, the RMS errors of fg-departures for channels that receive a greater contribution from the surface are much smaller for experiment-dyn and experiment-skin than for the SSMI/S control. Figure 16 displays time series of the RMS error of fg-departures obtained over land at (a) 52.8, (b) 22 and (c) 150 GHz and from the control (solid lines) and experiment-dyn (dashed lines). The latter two SSMI/S surface channels are

not assimilated within both experiments. Fg-departure RMS error for surface sensitive SSMI/S observations are globally improved with updated emissivities. The improvement of RMS error is very significant. The RMS error changes from nearly 7 K (control) to 2 K and from 11 K (control) to 2.5 K for channels 14 (22.2-V GHz) and 8 (150-V GHz) respectively.

b) Forecast impact

The forecast performances of the control, experiment-dyn and experiment-skin have been compared. A small positive impact on forecasts of the geopotential height over the Southern Hemisphere has been observed when SSMI/S temperature sounding channels are assimilated over land (experiment-dyn). However, the impact of SSMI/S over land from experiment-dyn seems to be neutral over the Northern Hemisphere. The Figure 17 shows the correlation between the 500 hPa geopotential height anomalies of the forecasts and the verifying analyses with the forecasts; the forecasts being verified against the operational analyses for the whole assimilation period (32 forecasts). The figure shows the improvement in forecasts with Experiment-dyn for the Southern hemisphere (Bottom) and the neutral impact over the Northern Hemisphere. Figure 18 shows a small improvement in forecasts with experiment-skin (against the control) for the Southern and the Northern hemispheres for the 500 hPa geopotential height forecasts. For experiment-dyn and experiment-skin, the forecast improvements over the Southern Hemisphere are significant at the 90% confidence level or better for a forecast range beyond 6. These results indicate that the information content of SSMI/S temperature sounding channels over land is more beneficial to the assimilation system when the surface is constrained by emissivity and /or skin temperature. Additional tests should be done in order to investigate the effect of a revised bias correction that takes into account land/sea differences. The neutral effect of SSMI/S assimilation over the Northern Hemisphere should be also investigated.

4.3. 4D-VAR AMSU-A & AMSU-B assimilation results

a) Model fit to the observations

The AMSU control experiment and experiment-dyn1 (see Table 4) use the same AMSU-A and AMSU-B channels over land. The only difference between the two experiments is the land emissivity. For the control experiment, emissivities at 50 GHz and at 89 GHz are determined using a regression and empirical models (Weng et al. 2001, Grody 1988). For the experiment-dyn1, emissivities are directly derived from satellite observations at 37 GHz and at 89 GHz for AMSU-A and AMSU-B respectively.

Globally, the fit of observations including AMSU against the First Guess and the analysis is not degraded for experiment-dyn1 compared with the control experiment. Figure 19 and Figure 20 show the statistics for the FG (solid) and the analysis departures (dashed) for the assimilated observations within the control (red) and the experiment-dyn1 (black) for AMSU-A and AMSU-B respectively. Results are given for the Northern Hemisphere in terms of standard deviations, biases and number of assimilated observations. We note an increase of up to 18 % in the number of assimilated observations for AMSU-A channels 5, 6, 7 with experiment-dyn1 with respect to the control. Similar results have been obtained for AMSU-B channels with an increase of about 28 % for channel 3 AMSU-B. Note that the experiments use a check on the First Guess departures of the window channels 4 for AMSU-A (absolute departures should be below 0.7 K) and 2 for AMSU-B/MHS (absolute departures should be below 5.0 K) to identify data with too strong cloud contamination for the lower-peaking channels. The updated emissivities in experiment-dyn1 will result in tighter histograms of FG

departures as noted earlier, thus leading to more data considered cloud-free over land in this experiment. This also contributes to the larger number of observations assimilated in experiment-dyn1.

b) Forecast impact

The forecast performances of the control experiment compared to the experiment-dyn1 indicate that a positive impact on forecast of the geopotential height and temperature occur over the Southern Hemisphere. The impact is statistically significant (90% of confidence level) at levels ranging from 1000 hPa to 200 hPa. The impact over the Northern Hemisphere is almost neutral. Figure 21 shows the correlation between the 500 hPa geopotential height anomalies of the forecasts and the verifying analyses with the forecasts; the forecasts being verified against their own analyses for the whole assimilation period (32 forecasts). Results are given for experiment-dyn1 (blue), the control experiment (red), the Northern Hemisphere (top) and the Southern Hemisphere (bottom). Figure 22 shows the improvement in forecasts with Experiment-dyn1 with respect to the control experiment for the Southern hemisphere and for the 1000 hPa (top), the 850 hPa (middle) and the 500 hPa (bottom) geopotential heights. The forecast improvements over the Southern Hemisphere are significant at the 90% confidence level or better for a forecast range beyond 5.

CONCLUSIONS

This paper reports on feasibility studies conducted at ECMWF in order to prepare the assimilation of microwave observations over land. The assimilation experiments use observations from SSMI/S temperature sounding channels with land emissivities and/or skin temperatures estimated from a selection of SSMI/S surface channels. Prior to the assimilation experiments, land emissivities have been calculated using 2 weeks of SSMI/S surface sensitive observations. Moreover, land emissivities have also been calculated at many frequencies using observations coming from SSMI, AMSRE, TMI, AMSU-A and AMSU-B. The consistency of SSMI/S land emissivities has been checked in terms of frequency and spatial dependencies. For all frequencies, SSMI/S emissivities have been found to be in good agreement with emissivities coming from the other microwave sensors. A slight positive bias was observed for SSMI/S emissivities at low frequencies compared with SSM/I ones. However, this bias is likely due to the flagging procedure which is applied to SSMI/S observations in order to remove observations contaminated by solar intrusions. In addition, the brightness temperature variation over land for surface-sensitive channels is artificially reduced, as a consequence of the flagging, and also as a result of the averaging over scales of around 118 km that has been performed in the SSMI/S data used here. Land SSMI/S Tbs from channels that receive a weak or a strong contribution from the surface have been simulated using emissivities calculated at selected frequencies. These simulations have been found to be in good agreement with observations.

Then several assimilation experiments have been run in order to investigate the impact of assimilating SSMI/S temperature sounding channels over land. The land emissivity and/or skin temperature have been calculated using a selection of SSMI/S surface channels. The impact of these experiments with respect to the control has been studied. The model fit to all observations was not altered by adding many SSMI/S data over land. The forecast scores have been found to be positive in the Southern Hemisphere and neutral in the Northern Hemisphere. These results are very encouraging and suggest that it is possible to take advantage of the information content of SSMI/S observations over land if an adequate modelling of the emissivity/or skin temperature is introduced. These results are nevertheless preliminary and need to be validated by other experiments over longer assimilation periods

and different seasons. Areas that require further attention are the bias correction over land, the performance of the cloud detection, and general quality control. Also, the use of humidity sounding and SSMI-like channels from SSMI/S over land could be investigated.

In addition to the SSMI/S experiments, other experiments have been run using AMSU-A and AMSU-B observations over land. Overall, the fg-departures for these experiments are improved when the land surface emissivity has been changed. The forecast scores have been calculated for an experiment with dynamically updated AMSU emissivities against a control experiment. A positive impact has been observed over the Southern Hemisphere for the geopotential and the temperature from 1000 to 300 hPa. The results are consistent with earlier findings (Gerard et al. 2006, Karbou et al. 2006b). Other experiments are planned over different seasons in order to derive final conclusions.

ACKNOWLEDGEMENTS

This study was partly funded by the NWP-SAF.

REFERENCES

1. Bell, W., S. English, B. Candy, N. Atkinson, F. Hilton, S. Swadley, B. Campbell, N. Bormann, G. Kelly and M. Kazumori, 2007, The assimilation of SSMI/S radiances in numerical weather prediction models, *IEEE Trans. On Geoscience and Remote sensing*, under revision.
2. Choudhury, B. J., Reflectivities of selected land surface types at 19 and 37 GHz from SSM/I observations, *Remote Sens. Environ.*, vol. 46, Issue 1, pp. 1-17, 1993.
3. Deblonde, G., and S. English, 2000, Evaluation of fastem and fastem2 fast microwave oceanic surface emissivity model. Proceeding of the 11th International ATOVS study conference, Budapest, Hungary, 67-78
4. English, S., D. Jones, A. Smith, F. Hilton, and K. Whyte, 2003, ATOVS and SSMI assimilation at the Met Office, *Proc. Of the thirteenth International TOVS study conference*, Sainte-Adèle, Canada.
5. Eyre, J. R., 1991, A fast radiatif transfer model for satellite sounding systems. *ECMWF Tech. Memo.*, 176, 28 pp.
6. Felde, G. W., and J. D. Pickle, "Retrieval of 91 and 150 GHz Earth surface emissivities," *J. Geophys. Res.*, vol. 100, NO. D10, pp 20,855-20,866, Oct 1995.
7. Grody, N. C., 1988, Surface identification using satellite microwave radiometers, *IEEE Trans. On Geoscience and Remote sensing*, 26, 850-859.
8. Guillou, C., W. Ellison, L. Eymard, ~K. Lamkaouci, C. Prigent, G. Delbos, G. Balana, and S. A. Boukabara, 1998, Impact of new permittivity measurements on sea surface emissivity modelling in microwaves. *Radio Science*, 33, 649-667.
9. Guissard, A., and P. Sobieski, 1987, An approximate model for the microwave brightness temperature of the sea. *Int. J. Remote Sens.* 8, 1607-1627.
10. Jones, A. S., and T. H. Vonder Haar, 1997, Retrieval of microwave surface emittance over land using coincident microwave and infrared satellite measurements, *J. Geophys. Res.*, vol. 102, NO. D12, pp 13,609-13,626, Jun 1997.
11. Karbou, F., E. Gérard, and F. Rabier, 2006a, Microwave land emissivity and skin temperature for AMSU-A and -B assimilation over land, *Q. J. R. Meteorol. Soc.*, ref. 05/216, vol. 132, No. 620, Part A, pp. 2333-2355(23).
12. Karbou, F., E. Gérard, and F. Rabier, 2006b, Impact of Improved Microwave Land Surface Emissivities in the 4D-Var system at Météo-France, 1st Workshop on Remote Sensing and Modelling of Surface Properties, 20-22 June 2006, Paris.

13. Karbou, F., C. Prigent, L. Eymard and J. Pardo, 2005, Microwave land emissivity calculations using AMSU-A and AMSU-B measurements. *IEEE Trans. on Geoscience and Remote Sensing*, 43, 5, 948-959.
14. Gérard, E., F. Karbou, F. Rabier and Z. Sahlaoui, Status of ATOVS and SSM/I data in the operational assimilation system at Météo-France and perspectives towards the use of microwave surface sensitive channels from ATOVS and SSM/I instruments over land, ITSC-XV: Maratea, Italy, 4-10 October 2006.
15. Kelly, G., and P. Bauer, 2000, The use of AMSU-A surface channels to obtain surface emissivity over land, snow and ice for Numerical Weather Prediction, *Proc. Of the Eleventh International TOVS study conference*, Budapest, Hungary, 167-179.
16. Matricardi, M., F. Chevallier, G. Kelly, and J. N. Thépaut, 2004, An improved general fast radiative transfer model for the assimilation of radiance observations. *Q. J. R. Meteorol.*, 130, 153-173.
17. Morland, J. C., David I. F. Grimes and T. J. Hewison, "Satellite observations of the microwave emissivity of a semi-arid land surface," *Remote Sens. Environ.*, vol. 77, Issue 2, pp. 149-164, 2001.
18. Morland, J. C., David I. F. Grimes, George Dugdale and Tim J. Hewison, "The Estimation of Land Surface Emissivities at 24 GHz to 157 GHz Using Remotely Sensed Aircraft Data," *Remote Sens. Environ.*, vol. 73, Issue 3, pp. 323-336, 2000.
19. Prigent, C., P. Abba, 1990, Sea surface equivalent brightness temperature at millimeter wavelength. *Annales Geophysicae*, 8, 627-634.
20. Prigent, C., W. B. Rossow, and E. Matthews, 1997, Microwave land surface emissivities estimated from SSM/I observations, *J. Geophys. Res.*, 102, 21867-21890.
21. Prigent, C., F. Chevallier, F. Karbou, P. Bauer and G. Kelly, 2005, AMSU-A surface emissivities for numerical weather prediction assimilation schemes. *J. Applied Meteorology*, 44, 416-426.
22. Rabier, F., H. Jarvinie, E. Klinker, J. F. Mahfouf and A. Simmons, 2000, The ECMWF operational implementation of four dimensional variational assimilation. I: Experimental results with simplified physics. *Q. J. R. Meteorol. Soc.*, 126, 1143-1170.
23. Rosenkranz, P. W. and D. H. Staelin, 1972, Microwave emissivity of ocean foam and its effect on nadiral radiometric measurements. *J. Geophys. Res.*, 77, 6528-6538.
24. Rosenkranz, P., 2001, Retrieval of temperature and moisture profiles from AMSU-A and AMSU-B measurements, *IEEE Trans. On Geoscience and Remote sensing*, 39, 2429-2435.
25. Saunders, R. W., M. Matricardi, and P. Brunel, 1999, An improved fast radiative transfer model for assimilation of satellite radiance observations. *Quart. J. Roy. Meteor. Soc.*, 125, 1407-1425.
26. Uppala, S. M., P. W. Kallberg, A. J. Simmons et al., 2005, The ERA-40 Reanalysis. *Q. J. R. Meteorol.*, accepted for publication.
27. Veersé, F., and J. N. Thépaut, 1998, Multiple truncation incremental approach for four dimensional variational data assimilation, *Q. J. R. Meteorol. Soc.*, 124, 1889-1908.
28. Weng, F., B. Yan and N. Grody, 2001, A microwave land emissivity model, *J. Geophys. Res.*, vol. 106, NO. D17, pp 20,115-20,123.
29. Wentz, F., 1975, A two scale scattering model for foam-free sea microwave brightness temperatures. *J. Geophys. Res.*, 80, 3441-3446.

Table 1: SSMI/S channel characteristics (noise is from not-averaged data)

	Frequency (GHz)	Bandwidth per pass band (MHz)	Polarisation	Noise equivalent (K)
1	50.3	380.0	V	0.21
2	52.8	388.8	V	0.20
3	53.596	380.0	V	0.21
4	54.4	382.5	V	0.20
5	55.5	391.5	V	0.22
6	57.29	330.0	RC	0.26
7	59.4	238.8	RC	0.25
8	150.0	1642.0	H	0.53
9	183.31±6.6	1526.0	H	0.56
10	183.31±3.0	1019.0	H	0.39
11	183.31±1.0	512.5	H	0.38
12	19.35	355.0	H	0.35
13	19.35	356.7	V	0.34
14	22.235	407.5	V	0.45
15	37.0	1615.0	H	0.26
16	37.0	1545.0	V	0.22
17	91.65	1418.0	V	0.19
18	91.65	1411.0	H	0.19
19	63.28±0.28	2.72	RC	1.23
20	$\mu = 60.79 \pm 0.36$	2.70	RC	1.18
21	$\mu \pm 0.002$	5.16	RC	0.86
22	$\mu \pm 0.005$	10.48	RC	0.58
23	$\mu \pm 0.016$	29.28	RC	0.37
24	$\mu \pm 0.050$	106.3	RC	0.38

Table 2: Surface channel characteristics for SSM/I, AMSRE, TMI, AMSU-A and AMSU-B instruments

Channels	Frequency	Polarisation
SSM/I		
1	19.35	V
2	19.35	H
3	22.235	V
4	37.0	V
5	37.0	H
6	85.0	V
7	85.0	H
AMSRE		
1	6.9	V
2	6.9	H
3	10.65	V
4	10.65	H
5	18.7	V
6	18.7	H
7	23.8	V
8	23.8	H
9	36.5	V
10	36.5	H
11	89.0	V
12	89.0	H
TMI		
1	10.65	V
2	10.65	H
3	19.35	V
4	19.35	H
5	21.3	V
6	37.0	V
7	37.0	H
8	85.5	V
9	85.5	H
AMSU-A		
1	23.8	Mixed polarisation
2	31.4	Mixed polarisation
3	50.3	Mixed polarisation
15	89.0	Mixed polarisation
AMSU-B		
16	89.0	Mixed polarisation
17	150.0	Mixed polarisation

Table 3: Overview of SSMI/S assimilation experiments

Experiments	Emissivity	Surface temperature	Assimilated channels
Control	Operational	Operational	2-7 and 23-24 over sea
Experiment-dyn	- 50V for temperature sounding channels - 91V for humidity sounding channels - 19V&H for surface channels	Background	2-7 and 23-24 over sea and land
Experiment-skin	Atlas of averaged emissivities at all SSMI/S surface channels	Derived at 19V	2-7 and 23-24 over sea and land

Table 4: Overview of AMSU-A & AMSU-B assimilation experiments

Experiments	Emissivity	Surface temperature	Assimilated channels
Control	Operational	Operational	AMSU-A 5-14 & AMSU-B 3-5
Experiment-dyn1	- 37 GHz emissivities for AMSU-A channels - 89 GHz emissivities for AMSU-B channels	Same as control	Same as control

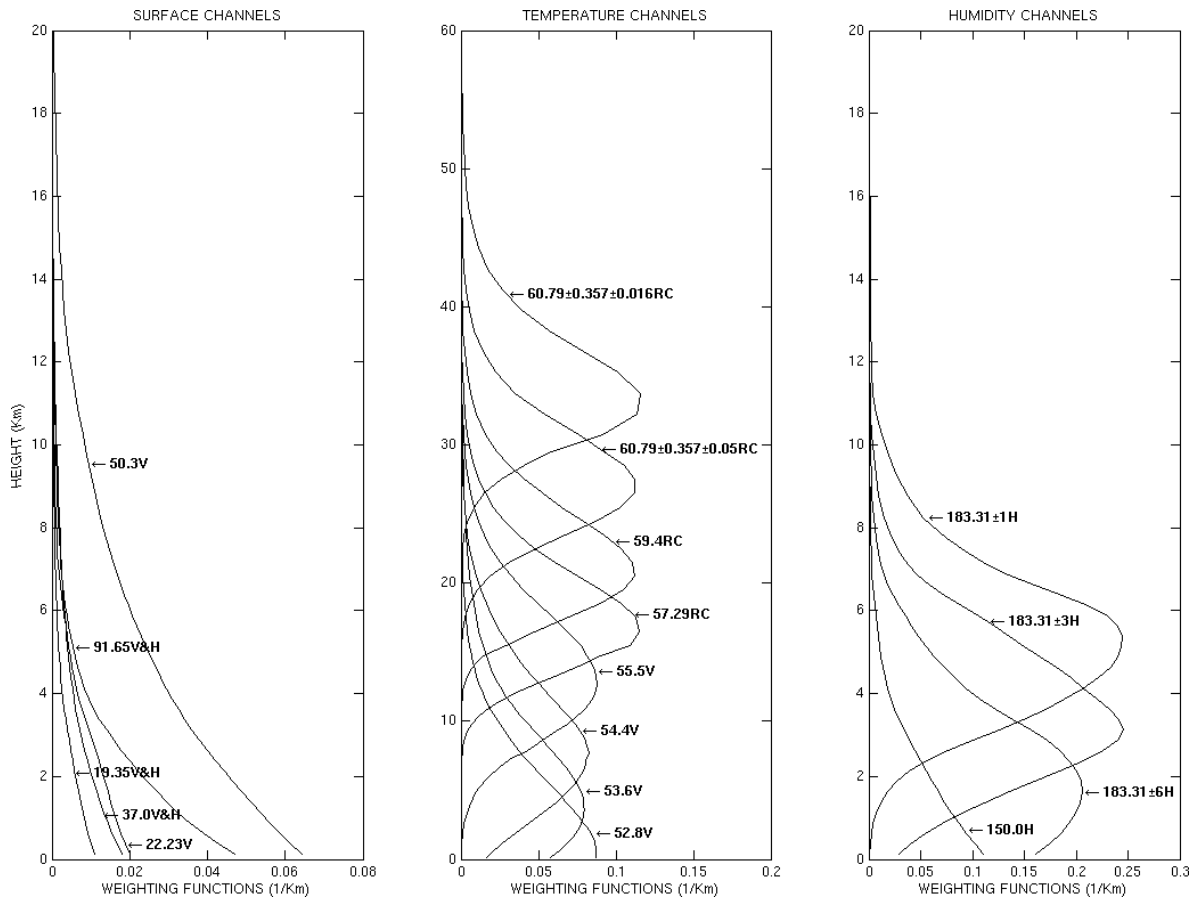


Figure 1: Weighting functions for a selection of SSMI/S channels and for a standard atmosphere

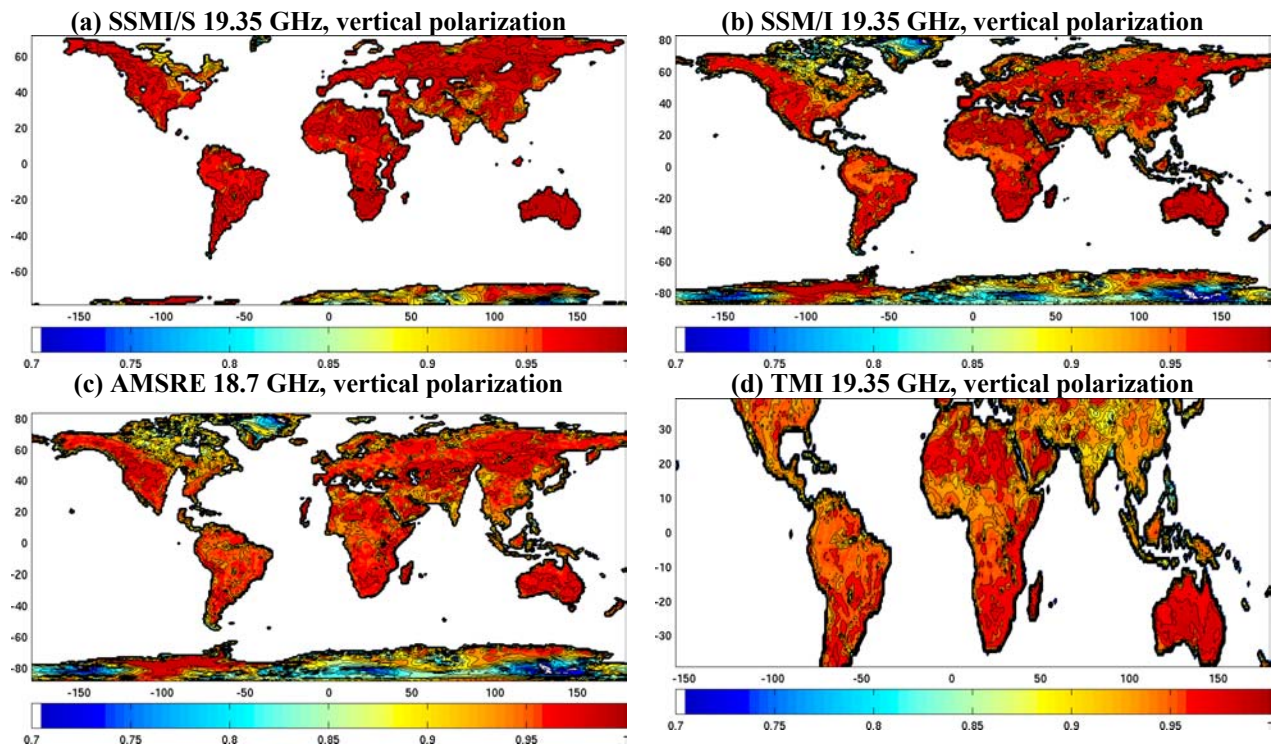


Figure 2: Mean land emissivity maps averaged over a two week period (from 2006-08-12 to 2006-08-25) and obtained from (a) SSMI/S 19-V, (b) SSM/I 19-V, (c) AMSRE 18-V, and (d) TMI 19-V channels

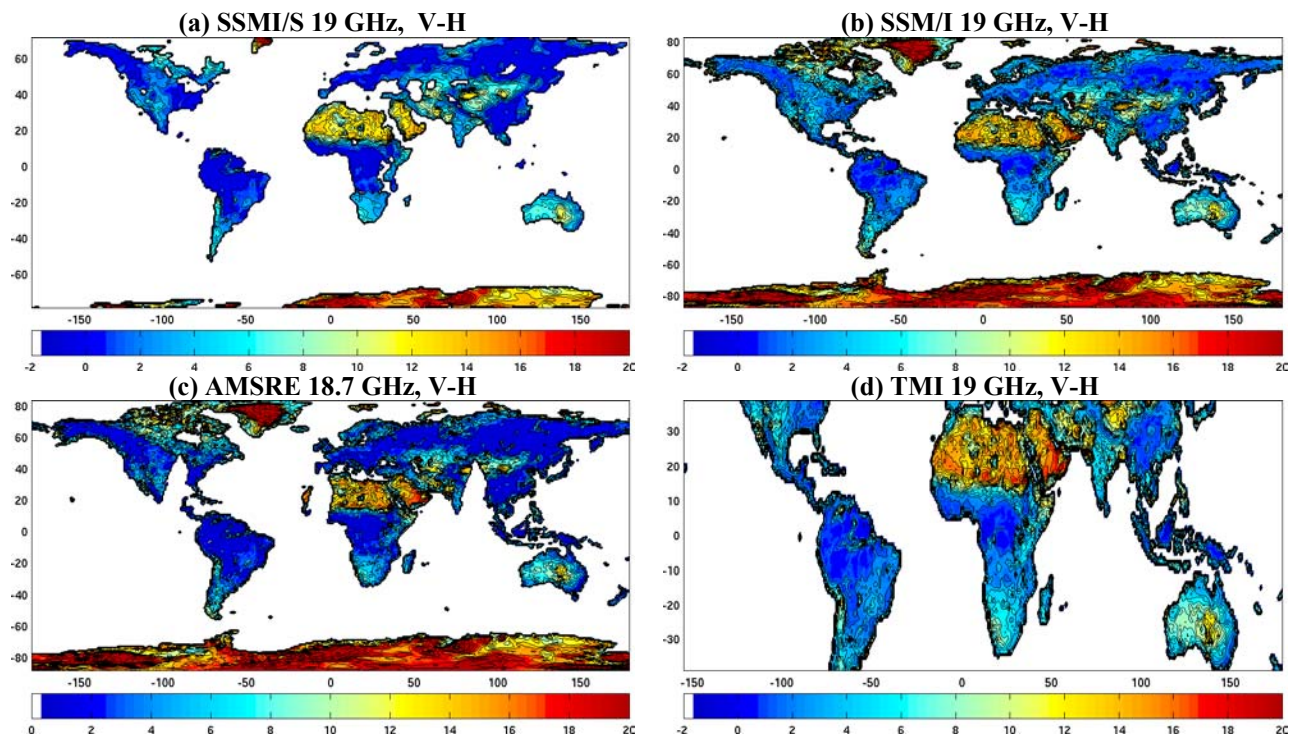


Figure 3: Mean land emissivity difference maps (V-H) in % averaged over a two week period (from 2006-08-12 to 2006-08-25) and obtained from (a) SSMI/S 19 GHz, (b) SSM/I 19 GHz, (c) AMSRE 18 GHz, and (d) TMI 19 GHz channels

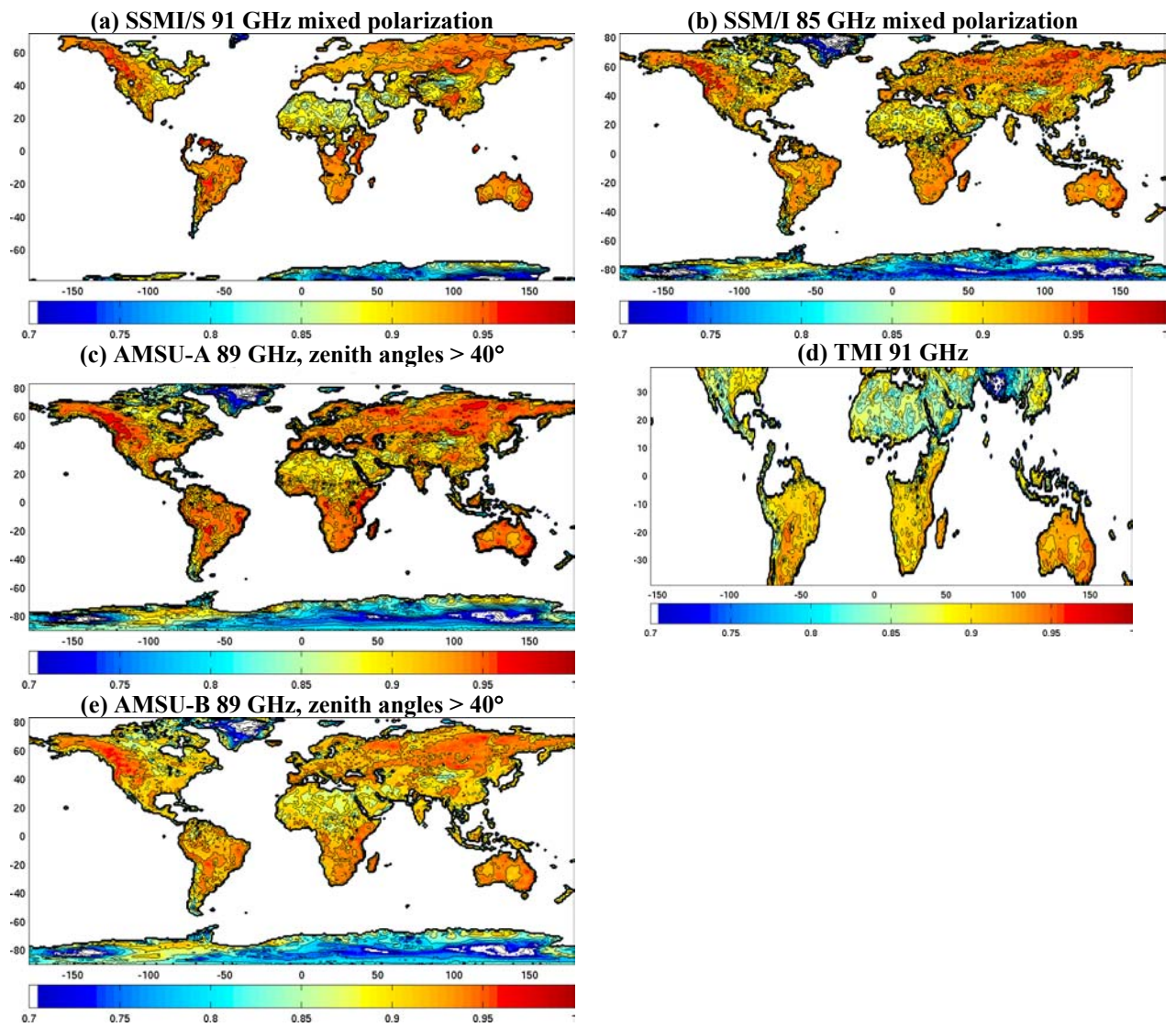


Figure 4: Mean land emissivity maps averaged over a two week period (from 2006-08-12 to 2006-08-25) and obtained from (a) SSMI/S 91, (b) SSM/I 85, (c) AMSU-A 89 GHz, (d) TMI 91 and (e) AMSU-B 89 GHz channels

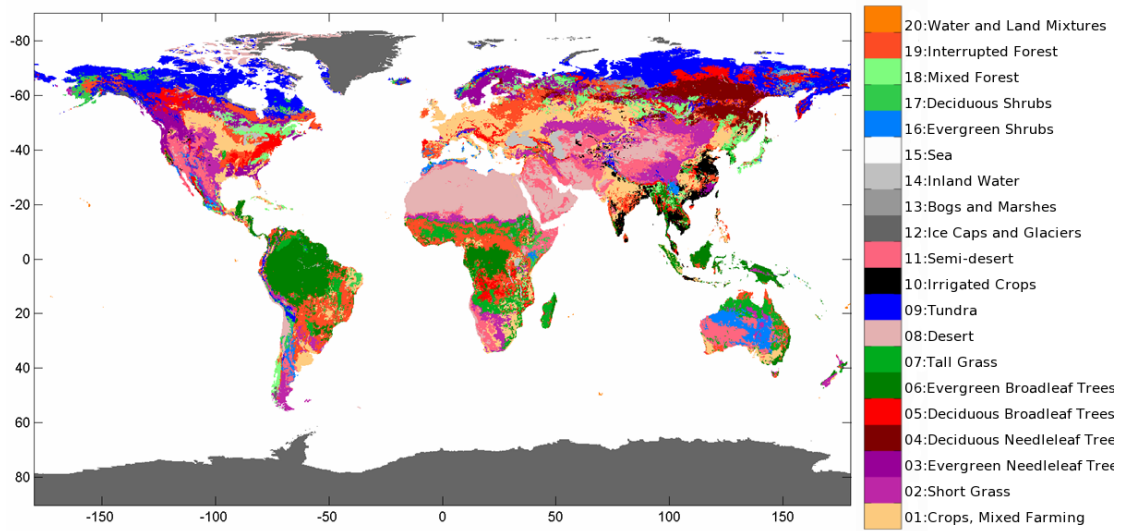


Figure 5: Biosphere-Atmosphere Transfer Scheme (BATS) surface types

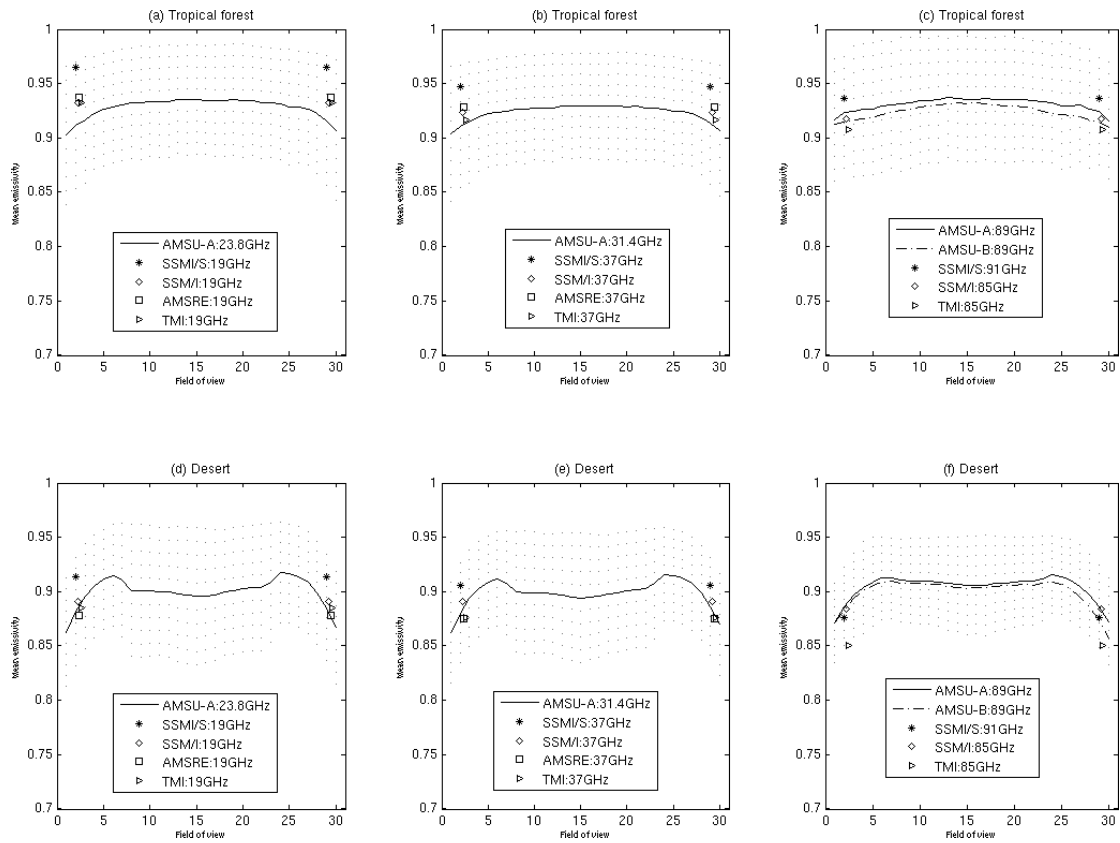


Figure 6: Mean land emissivities averaged over two weeks with respect to 30 scan position ($\pm 58^\circ$ of zenith angle variation) and two surface types: forest (a, b, c) and desert (d, e, f) surfaces. Results are given for frequencies close to 23, 31, and 91 GHz respectively and for observations coming from AMSU-A, AMSU-B, SSM/I, SSM/I/S, AMSRE and TMI.

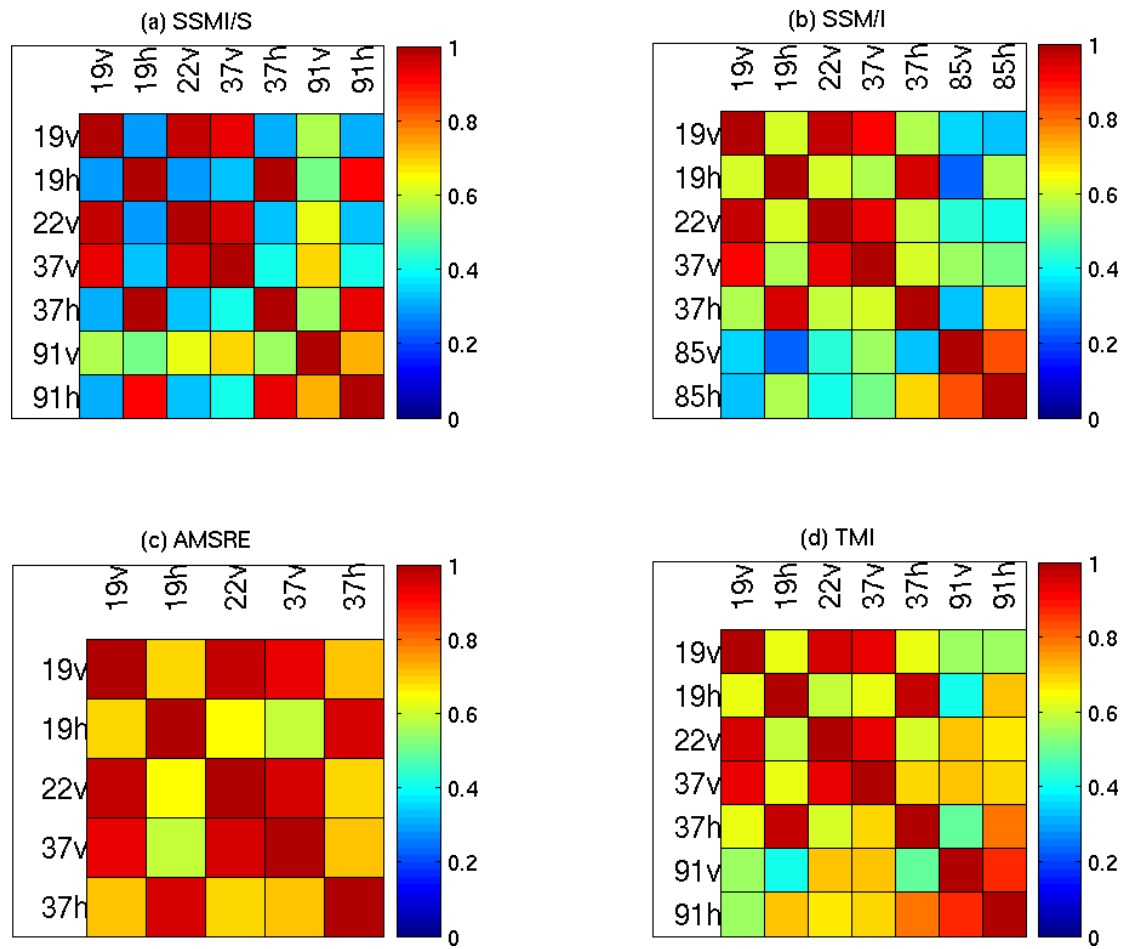


Figure 7: Land surface emissivity correlation coefficients obtained using surface channels from (a) SSMI/S, (b) SSM/I, (c) AMSRE, and (d) TMI.

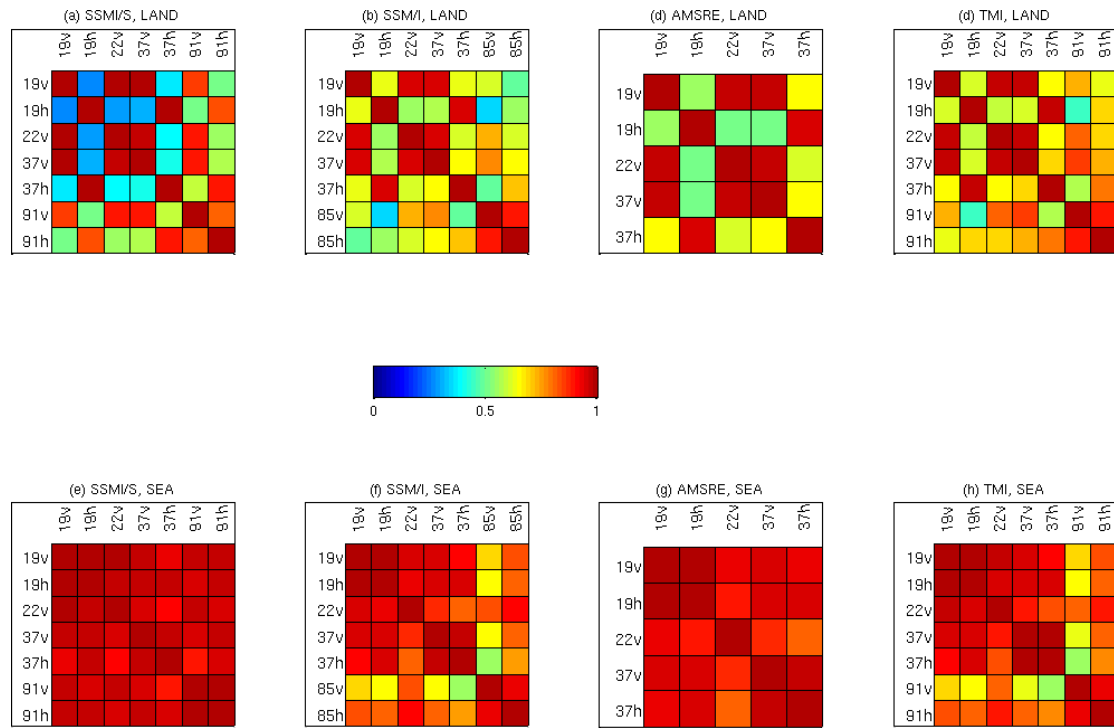


Figure 8: Brightness temperature correlation coefficients obtained using surface channels over land from (a) SSMI/S, (b) SSMI, (c) AMSRE, (d) TMI and over sea from the same instruments (e) to (h).

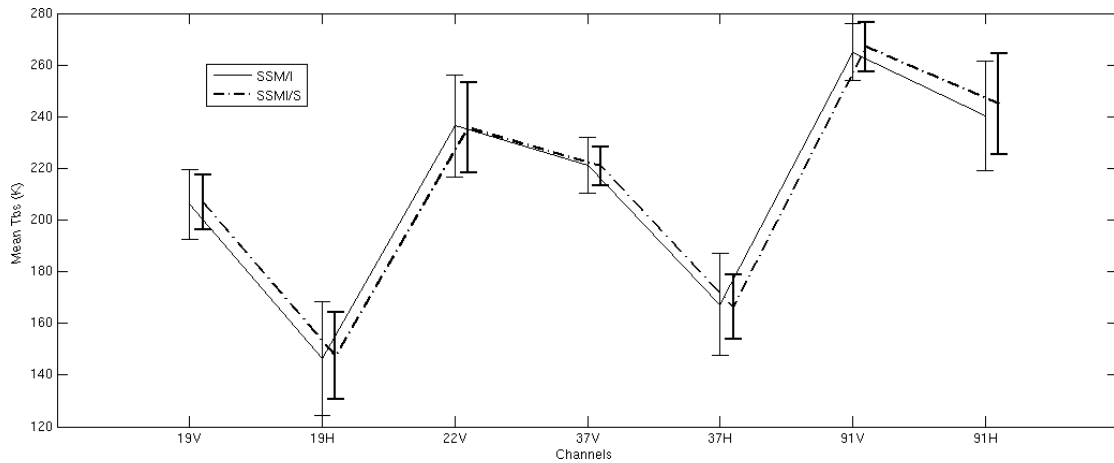


Figure 9: Mean Tbs values and standard deviations for SSMI/I (solid line) and SSMI/S (dashed line) surface channels obtained using 4 days of data over sea.

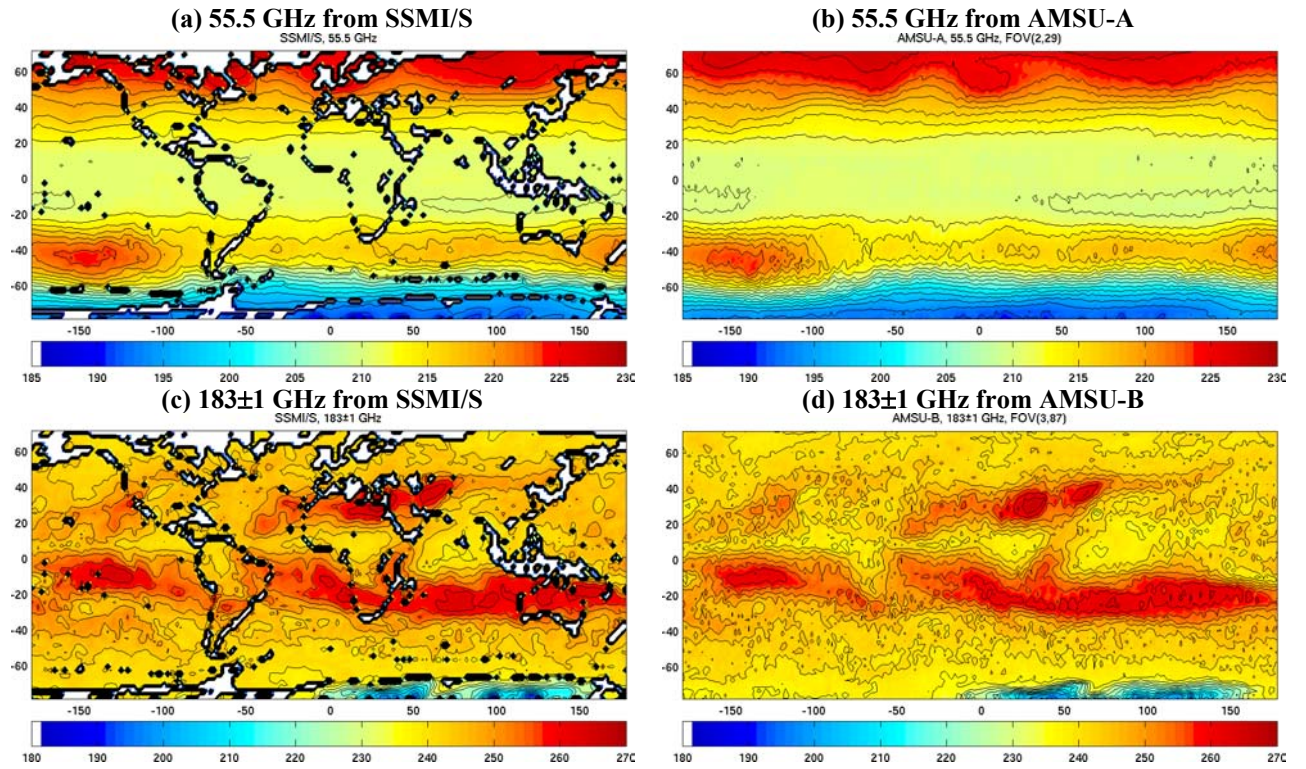


Figure 10: Mean brightness temperatures averaged over two weeks at (a) 55.5 GHz from SSMI/S, (b) 55.5 GHz from AMSU-A observations close to 53°, (c) 183±1 GHz from SSMI/S and (d) 183±1 GHz from AMSU-B observations close 53°.

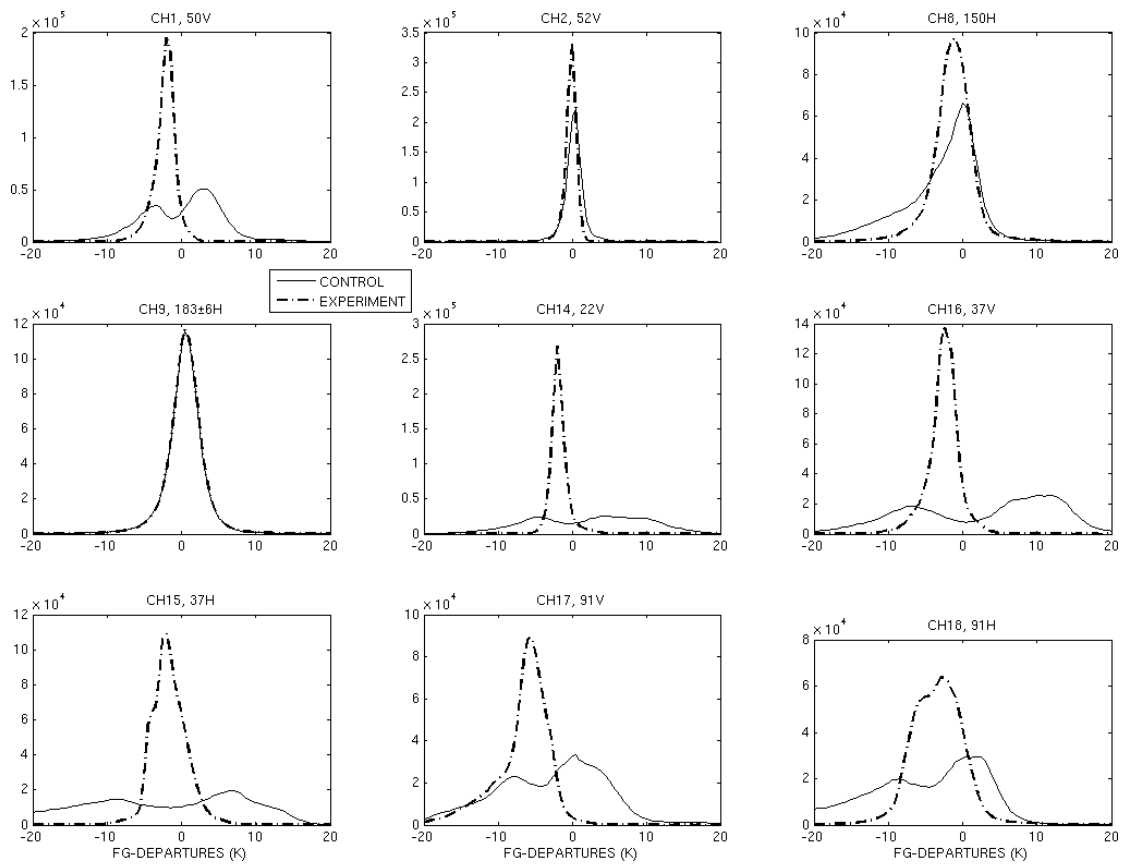


Figure 11: Histograms of fg-departures (without bias correction) obtained over land and for SSMI/S channels 1, 2, 8, 9, 14, 16, 15, 17 and 19. Results from the control and the experiment are shown as solid and dashed curves respectively.

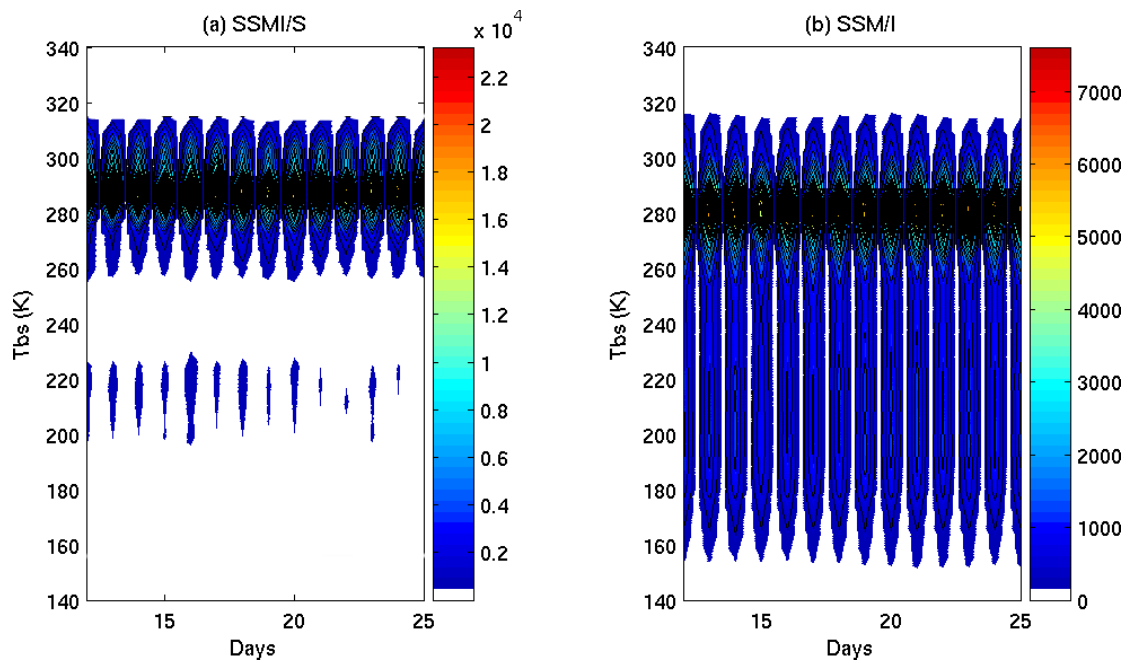


Figure 12: Scatter plots of brightness temperatures at 19-V GHz against observation days (from 12-08-2006 to 25-08-2006) and obtained for (a) SSMI/S and (b) SSM/I. The color bars indicate the number of observations per day.

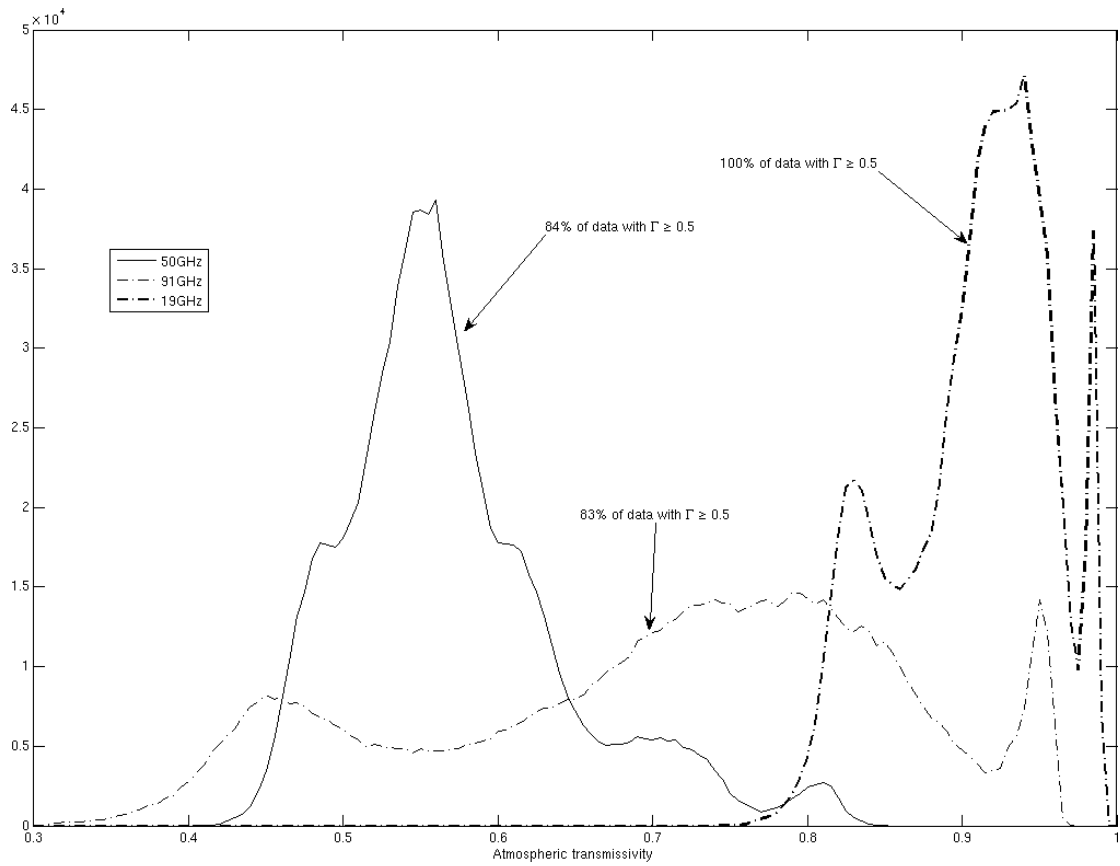


Figure 13: Atmospheric transmission histograms calculated using 2 weeks of data (12-08-06 to 25-08-06) and for the 50 GHz (solid curve), 91 GHz (dash-dotted curve) and 19 GHz (Bold dash-dotted curve).

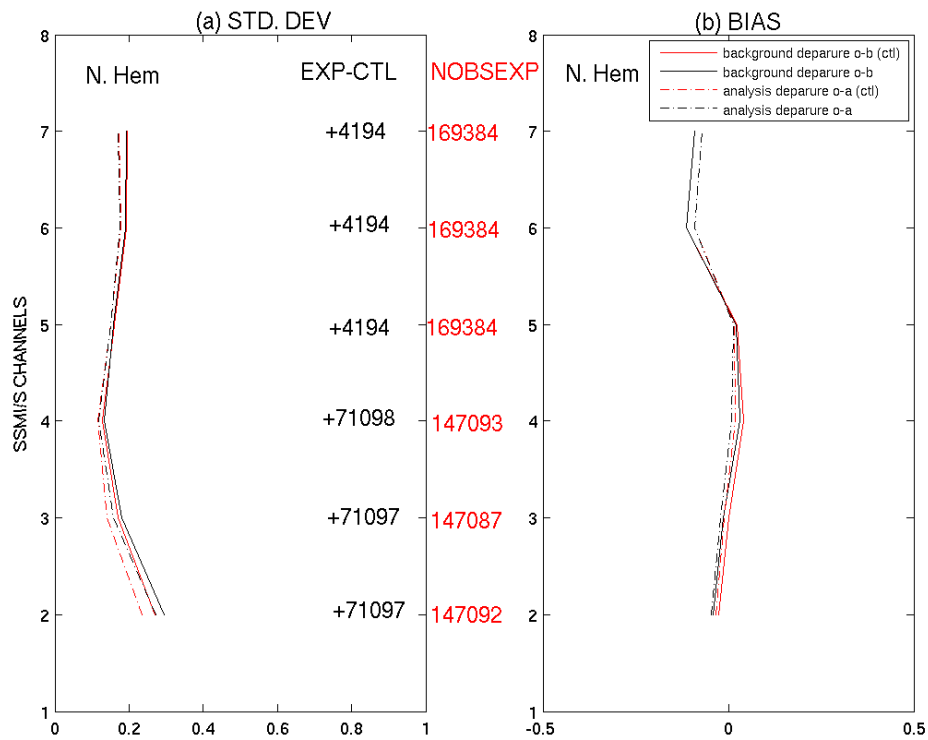


Figure 14: Statistics for the First Guess (solid) and the analysis departures (dashed) for used SSMI/S observations for the experiment-dyn (black) and the control (red). Panels (a) and (b) show the standard deviations (K) and the bias (K) versus SSMI/S channels respectively. The number of used SSMI/S observations in experiment-dyn is also shown (in red) as well as the difference EXP-CTL given in black.

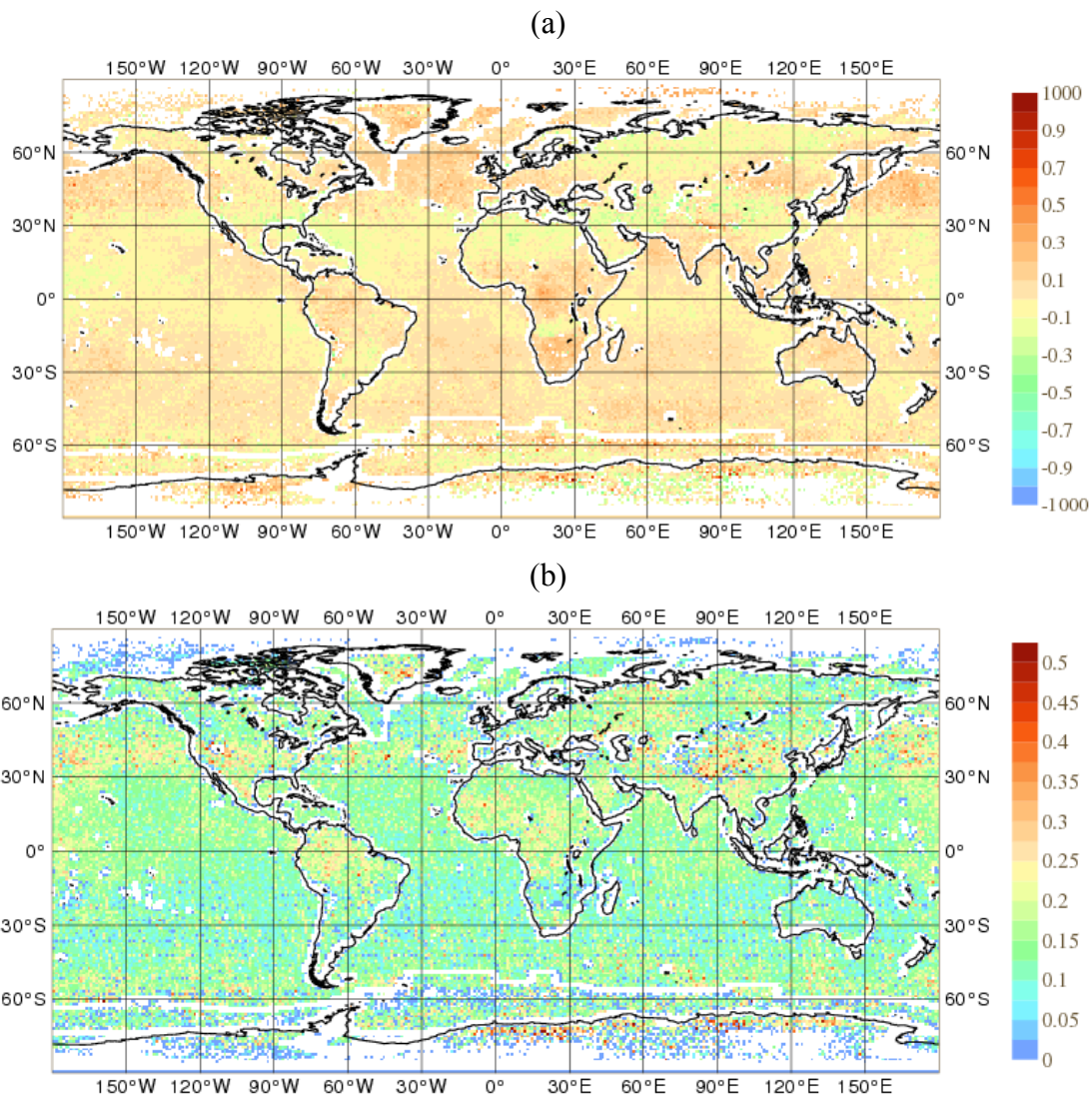


Figure 15: Statistics computed for bias-corrected radiances from SSMI/S channel 3 over 26 days (01/09/2006 to 26/09/2006) and from experiment-dyn; results are given for : (a) mean first guess departures (obs-guess) and (b) the corresponding standard deviations.

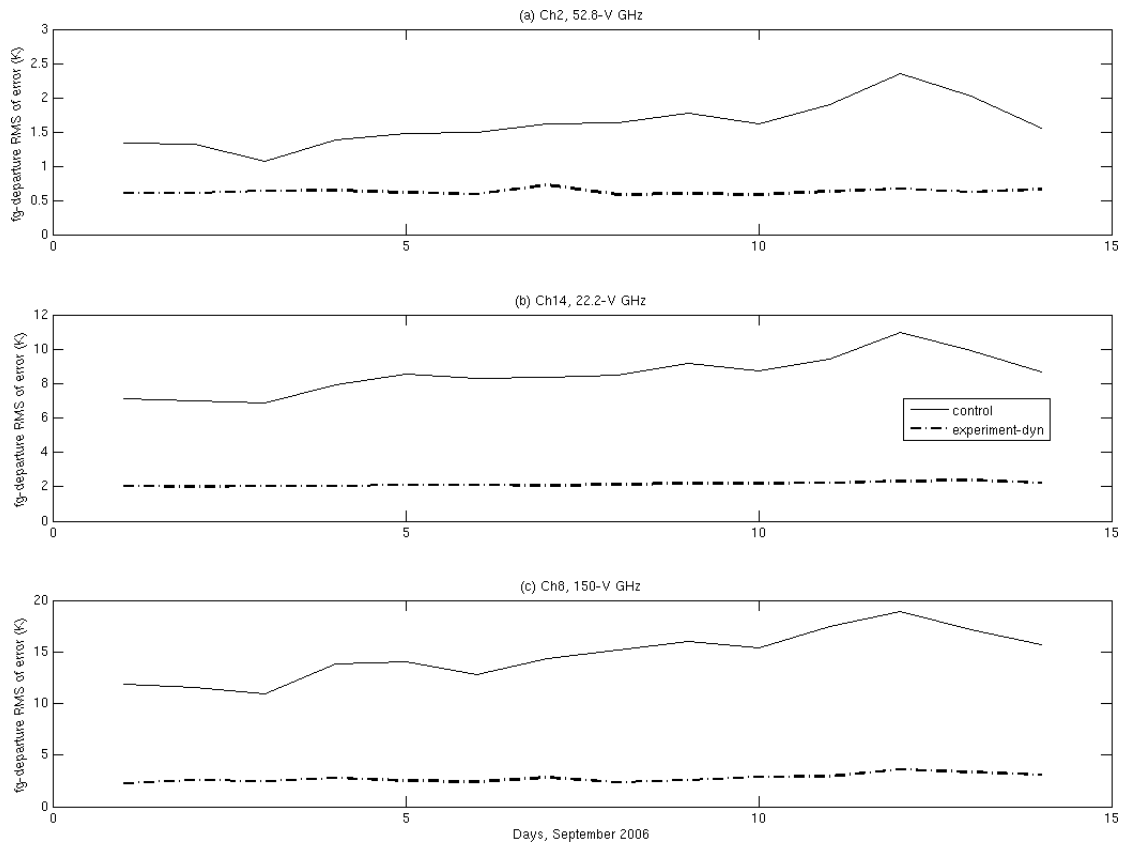


Figure 16: fg-departures (without bias correction) Root Mean Square error time series obtained over land and for SSMI/S channels 2, 14 and 8. Results from the control and the experiment are shown as solid and dashed curves respectively.

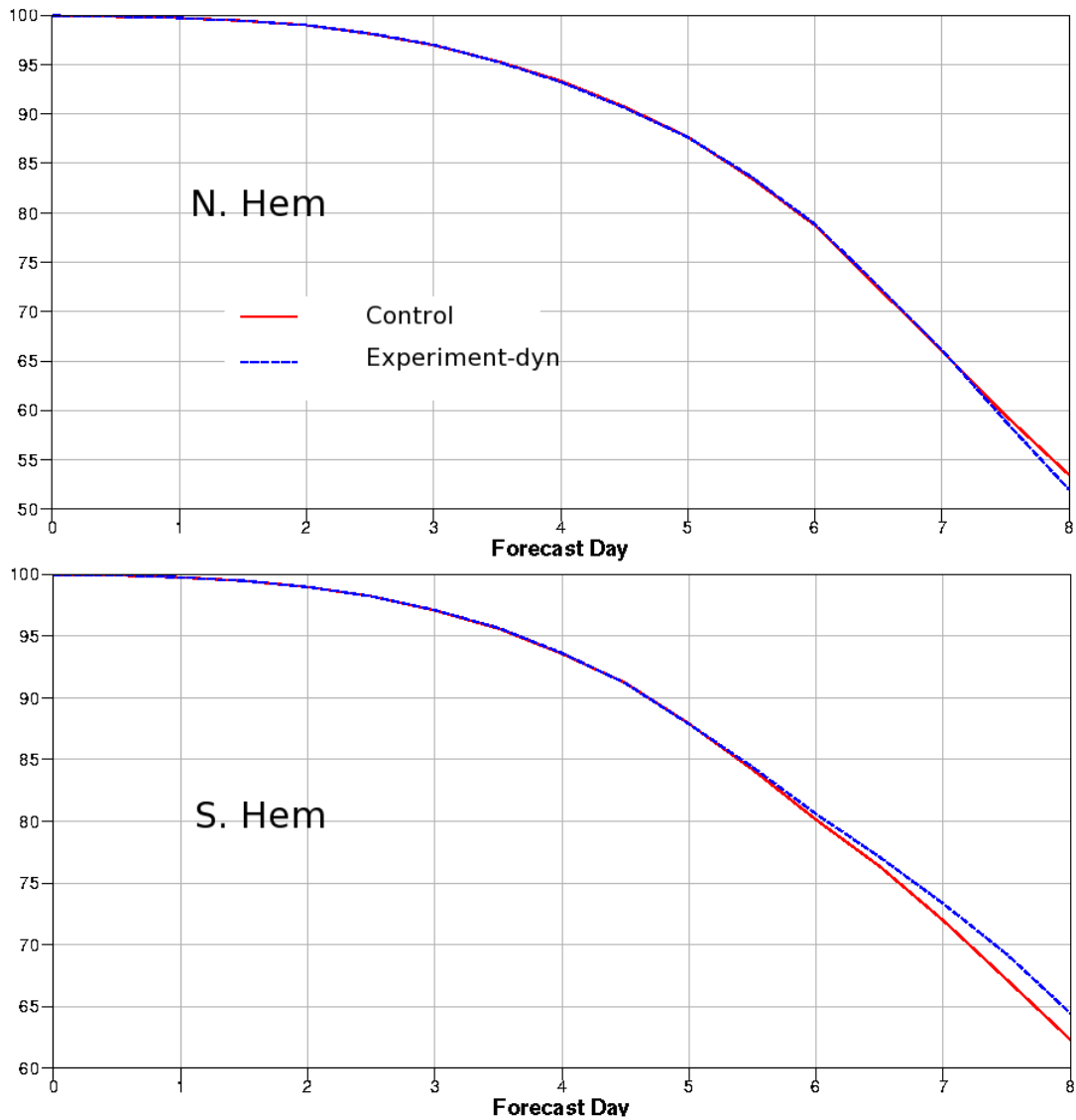


Figure 17: Anomaly correlation for the 500 hPa geopotential height forecast with respect to the verifying analysis as a function of forecast range and for the Northern Hemisphere (top) and the Southern Hemisphere (bottom). Results are given for the experiment-dyn that assimilates SSMI/S temperature channels over land and sea (blue curves) and for the control experiment. Scores have been calculated using the whole assimilation period (32 forecasts).

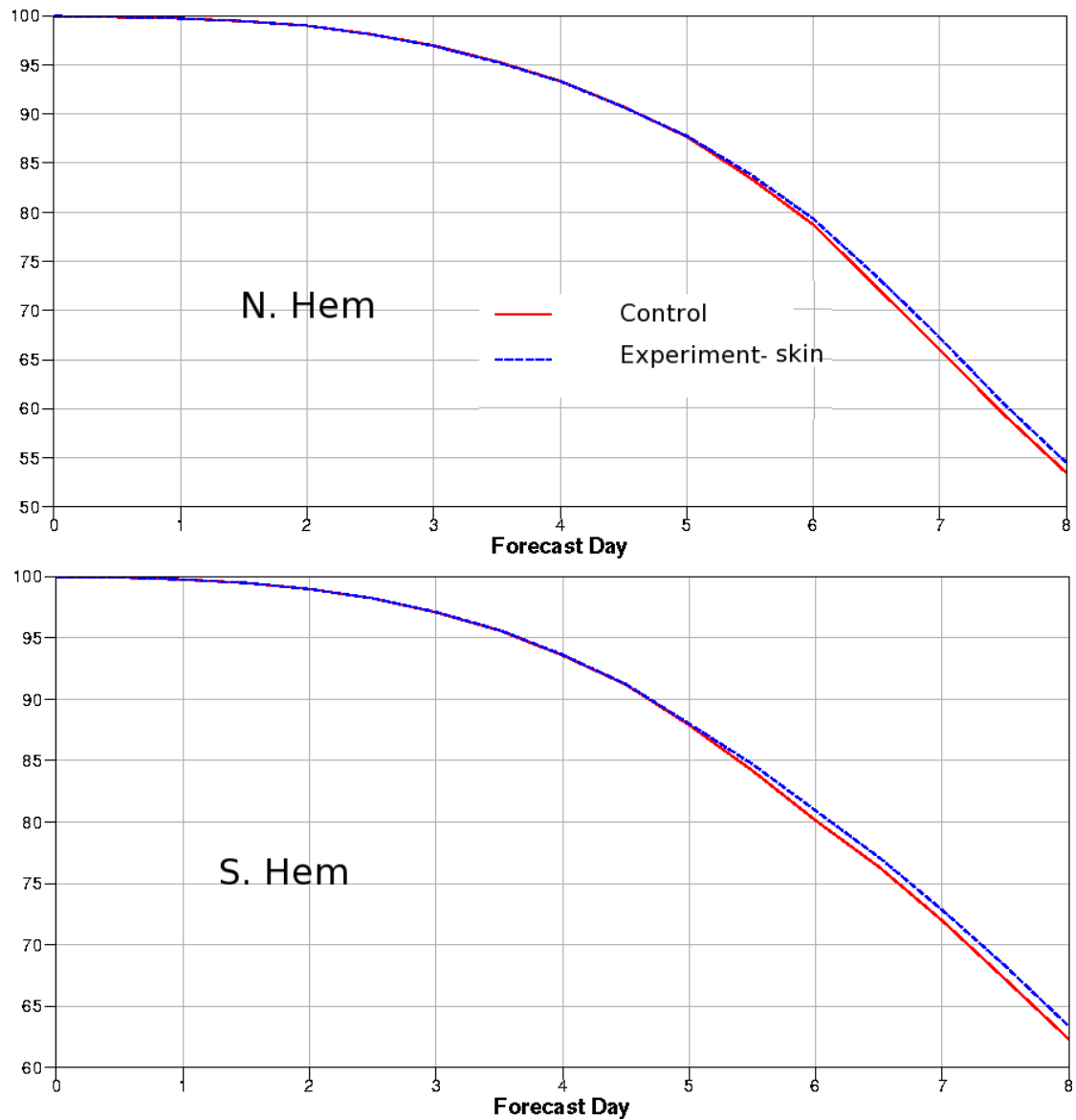


Figure 18: Anomaly correlation for the 500 hPa geopotential height forecast with respect to the verifying analysis as a function of forecast range and for the Northern Hemisphere (top) and the Southern Hemisphere (bottom). Results are given for the experiment-skin that assimilates SSMI/S temperature channels over land and sea (blue curves) and for the control experiment. Scores have been calculated using the whole assimilation period (32 forecasts).

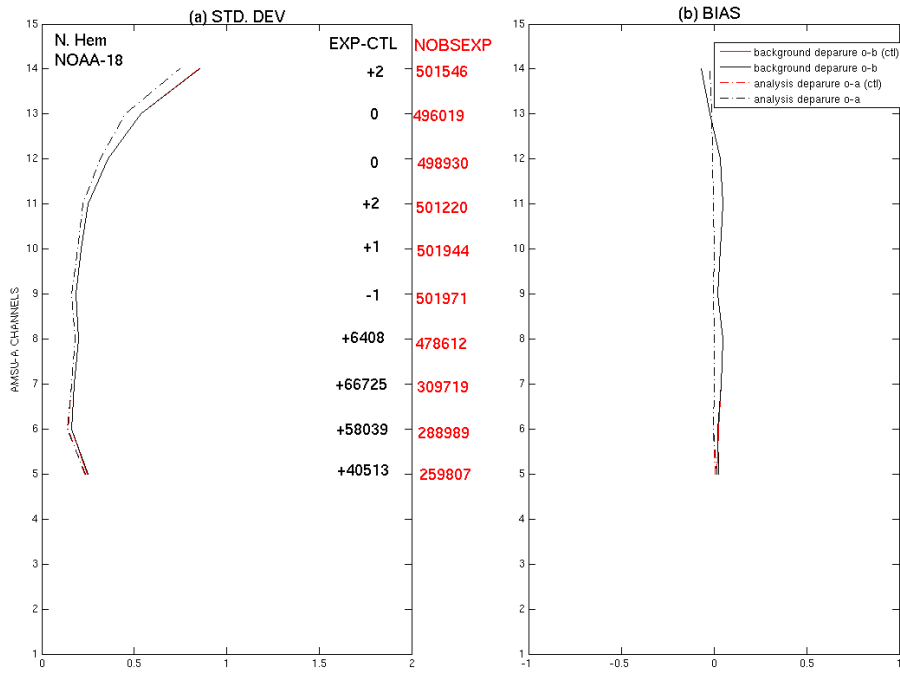


Figure 19: Statistics for the First Guess (solid) and the analysis departures (dashed) for used AMSU-A observations from NOAA-18 over the Northern Hemisphere for the experiment-dyn (black) and the control (red). Panels (a) and (b) show the standard deviations (K) and the bias (K) versus AMSU-A channels respectively. The number of used AMSU-A observations in experiment-dyn is also shown (in red) as well as the difference EXP-CTL given in black.

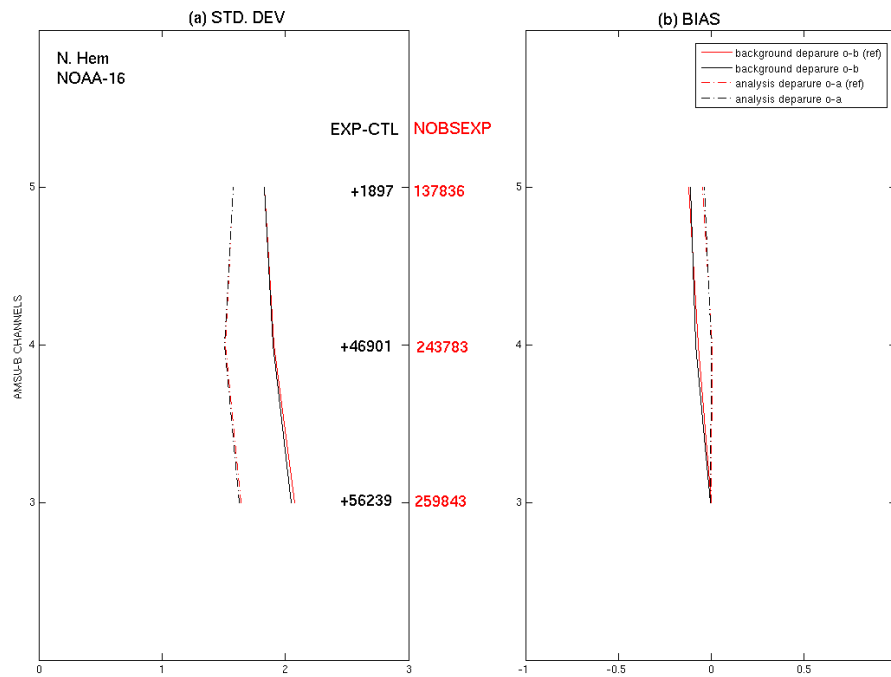


Figure 20: Statistics for the First Guess (solid) and the analysis departures (dashed) for used AMSU-B observations from NOAA-16 over the Northern Hemisphere for the experiment-dyn (black) and the control (red). Panels (a) and (b) show the standard deviations (K) and the bias (K) versus AMSU-B channels respectively. The number of used AMSU-B observations in experiment-dyn is also shown (in red) as well as the difference EXP-CTL given in black.

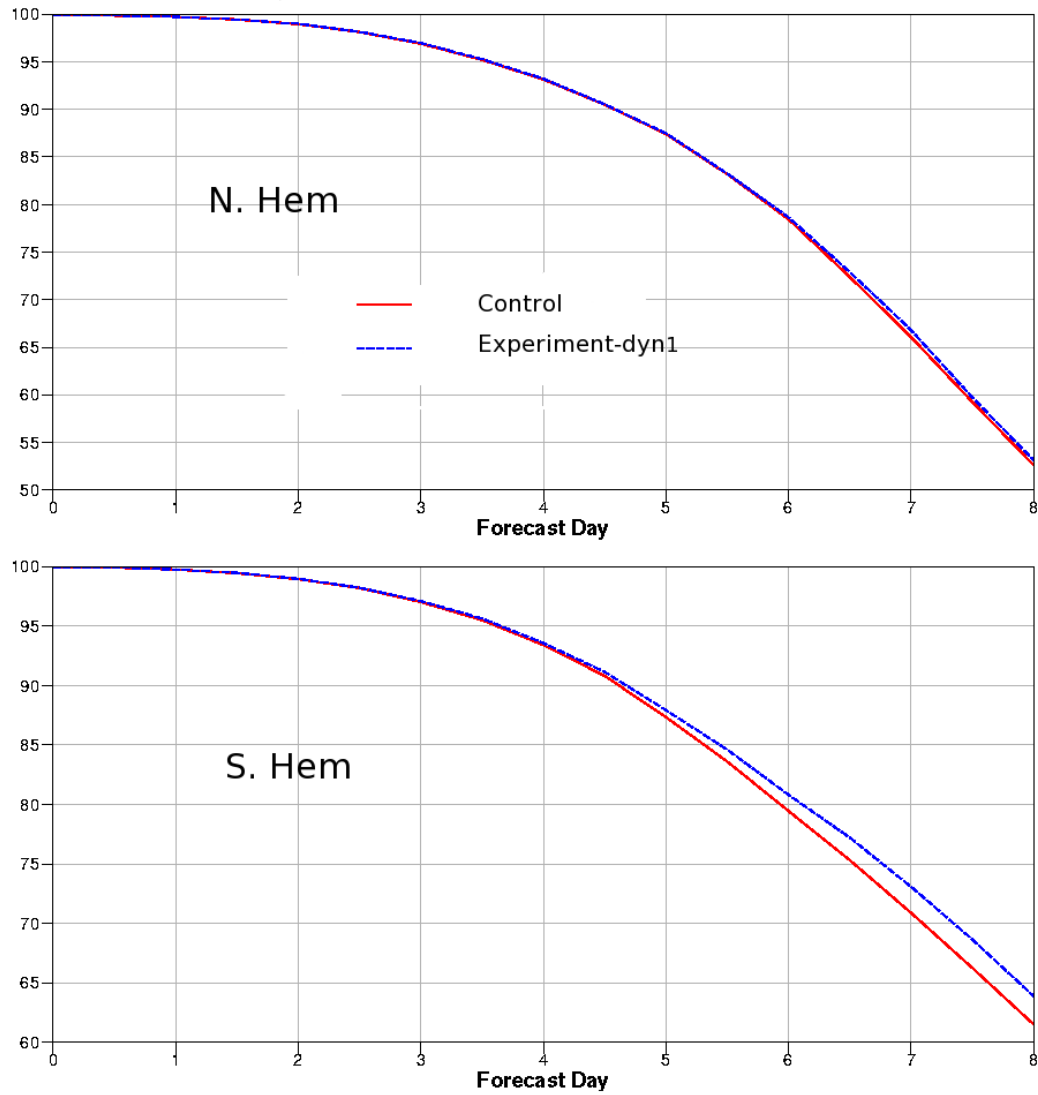


Figure 21: Anomaly correlation for the 500 hPa geopotential height forecast with respect to the verifying analysis as a function of forecast range and for the Northern Hemisphere (top) and the Southern Hemisphere (bottom). Results are given for the experiment-dyn that assimilates AMSU-A temperature channels over land and sea (blue curves) and for the control experiment. Scores have been calculated using 32 forecasts.

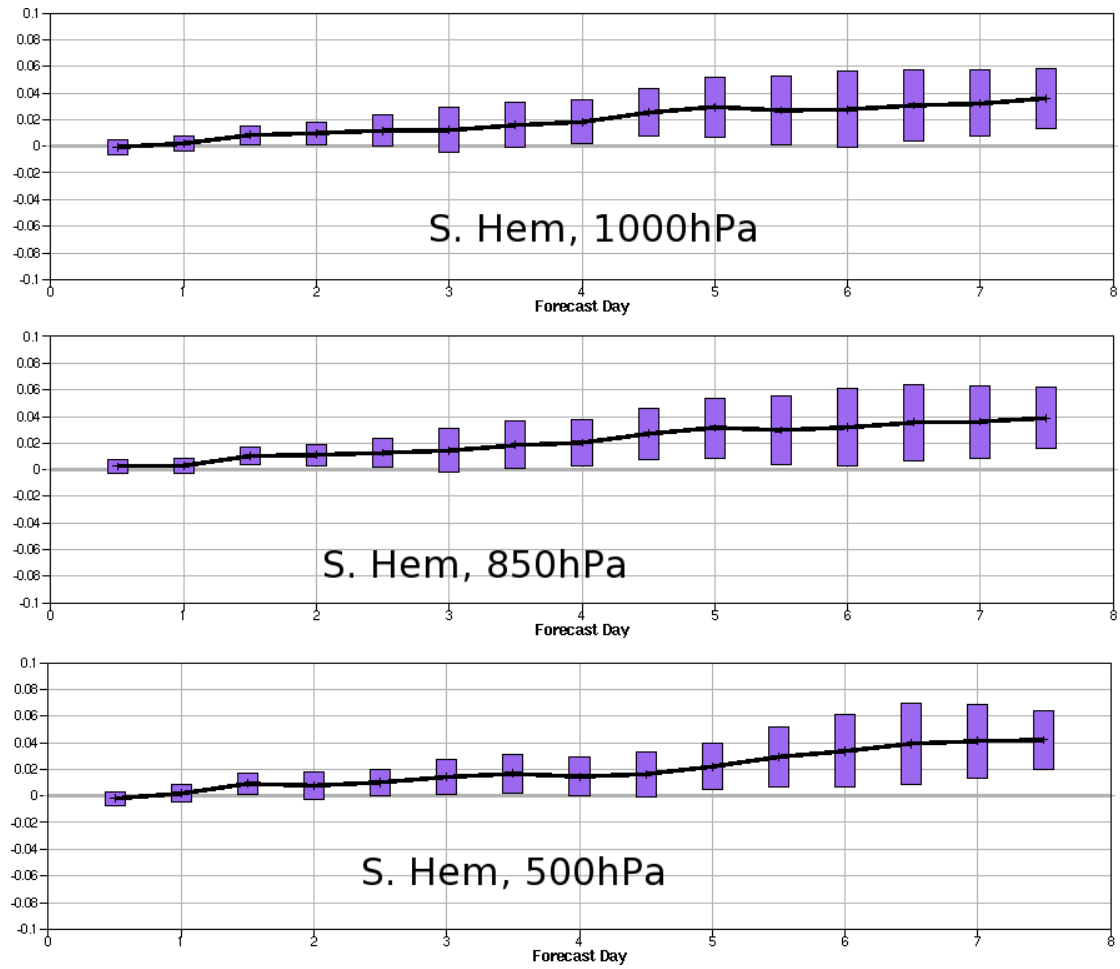


Figure 22: Mean normalized Root Mean Square error differences (Control-Experiment-dyn) for the geopotential height forecast with each experiment verified against their own analyses. Results are given for the Southern Hemisphere for the 1000 hPa (top), 850 hPa (middle), and 500 hPa (bottom) geopotential heights. Scores have been produced for a month period (32 forecast)